Dean, J.R., Jones, M.D., Leng, M.J., Noble, S.R., Metcalfe, S.E., Sloane, H.J., Sahy, D., Eastwood, W.J., Roberts, C.N. 2015. Eastern Mediterranean hydroclimate over the late glacial and Holocene, reconstructed from the sediments of Nar lake, central Turkey, using stable isotopes and carbonate mineralogy. *Quaternary Science Reviews* 124, 162-174.

Eastern Mediterranean hydroclimate over the late glacial and Holocene, reconstructed from the sediments of Nar lake, central Turkey, using stable isotopes and carbonate mineralogy

Jonathan R. Dean[a,b,c*], Matthew D. Jones[b,c], Melanie J. Leng[a,c], Stephen R. Noble[a], Sarah E. Metcalfe[b,c], Hilary J. Sloane[a], Diana Sahy[a], Warren J. Eastwood[d] and C. Neil Roberts[e]

[a]*NERC Isotope Geosciences Facilities, British Geological Survey, Nottingham NG12 5GG UK*

[b]*School of Geography, University of Nottingham NG7 2RD UK*

[c]*Centre for Environmental Geochemistry, University of Nottingham NG7 2RD UK*

[d]*School of Geography, Earth and Environmental Sciences, University of Birmingham B15 2TT UK*

[e]*School of Geography, Earth and Environmental Sciences, University of Plymouth PL4 8AA UK*

*Corresponding author, jonathan.dean@bgs.ac.uk +44 (0)7944 747013

Abstract

There is a lack of high-resolution records of hydroclimate variability in the Eastern Mediterranean from the late glacial and early Holocene. More knowledge of the speed of climate shifts and the degree to which they were synchronous with changes in the North Atlantic or elsewhere is required to understand better the controls on Eastern Mediterranean climate. Using endogenic carbonate from a sediment sequence from Nar Gölü, a maar lake in central Turkey, dated by varve counting and uranium-thorium methods, we present high-resolution (~25 years) oxygen ($\delta^{18}O$) and carbon isotope records, supported by carbonate mineralogy data, spanning the late glacial and Holocene. $\delta^{18}O_{carbonate}$ at Nar Gölü has been shown previously to be a strong proxy for regional water balance. After a dry period (i.e. evaporation far exceeding precipitation) in the Younger Dryas, the data show a transition into the relatively wetter early Holocene. In the early Holocene there are two drier periods that appear to peak at ~9.3ka and ~8.2ka, coincident with cooling 'events' seen in North Atlantic records. After this, and as seen in other records from the Eastern Mediterranean, there is a millennial-scale drying trend through the Mid Holocene Transition. The relatively dry late Holocene is punctuated by centennial-scale drought intervals, at the times of 4.2ka 'event' and Late Bronze Age societal 'collapse'. Overall, we show that central Turkey is drier when the North Atlantic is cooler, throughout this record and at multiple timescales, thought to be due to a weakening of the westerly storm track resulting from reduced cyclogenesis in the North Atlantic. However, some features, such as the Mid Holocene Transition and the fact the early Holocene dry episodes at Nar Gölü are of a longer duration than the more discrete 'events' seen in North Atlantic records, imply there are additional controls on Eastern Mediterranean hydroclimate.

Highlights

- Sub-centennial resolution late glacial and Holocene isotope record from Turkey
- Rapid transition from a dry late glacial into a wet early Holocene
- Drier anomalies apparently at times of 9.3ka and 8.2ka events but last longer at Nar
- Droughts at times of 4.2ka event and Late Bronze Age societal ‘collapse’
- Strong teleconnection with North Atlantic, but additional other drivers

Keywords

Oxygen and carbon isotopes; Eastern Mediterranean; lake sediment; Holocene; late glacial; Mid Holocene Transition; 9.3ka event; 8.2ka event; 4.2ka event; Late Bronze Age

1 Introduction

Water in the Eastern Mediterranean is a key and politically sensitive resource (Issar and Adar, 2010) with rain-fed agriculture impossible across much of the region and regional climate models suggesting conditions will become even drier through this century (Kitoh et al., 2008). An improved understanding of hydroclimate over long timescales, >100 years, can help identify the potential drivers of climate in the region under different boundary conditions, assisting in the long-term sustainable management of water resources. This link between people and their hydro-environment has been important for millennia, potentially influencing the rise and fall of civilisations (e.g. Issar and Zohar, 2007; Rosen, 2007).

Current knowledge of regional palaeoclimatology suggests a dry, cool period in the Eastern Mediterranean from ~12,900-11,700 years BP at the time of the Younger Dryas (Bar-Matthews et al., 1999; Wick et al., 2003; Jones et al., 2007; Castañeda et al., 2010; Kotthoff et al., 2011), followed by a wetter early Holocene marked by increased precipitation (Bar-Matthews et al., 1999; Jones et al., 2007; Verheyden et al., 2008; Ocakoğlu et al., 2013). There followed a significant shift in hydroclimate in the mid Holocene to a drier late Holocene: the so-called Mid Holocene Transition (review of lake isotope data; Roberts et al., 2008; 2011).

In the early Holocene in the North Atlantic region, two key centennial-scale cooling episodes, at ~9,300 years BP and ~8,200 years BP, are well documented (e.g. von Grafenstein et al., 1999; Rasmussen et al., 2006). These are expressed in many other northern hemisphere regions as cool and/or dry periods, for example at the time of the 9.3ka ‘event’ in China (Dykoski et al., 2005) and Oman (Fleitmann et al., 2003; 2007) and at the time of the 8.2ka ‘event’ in Turkey (Turner et al., 2008; Göktürk et al., 2011), Israel (Bar-Matthews et

al., 2003; Almogi-Labin et al., 2009), China (Dykoski et al., 2005) and Oman (Fleitmann et al., 2003; 2007)

Late Holocene records (e.g. Jones et al., 2006) and present day climate (e.g. Cullen and deMenocal, 2000; Harding et al., 2009) show clear links between the Eastern Mediterranean and both the North Atlantic and the Indian Summer Monsoon. However, there is a lack of records from the region with the required temporal resolution to allow for a thorough investigation of centennial-scale climate change, and hence teleconnections to other regions, beyond the late Holocene. To address this gap, we present a new, high-resolution (~25 years) oxygen ($\delta^{18}O$) and carbon ($\delta^{13}C$) isotope record, with carbonate mineralogy data, from Nar Gölü (Gölü = lake in Turkish) in central Turkey through the late glacial and Holocene. This allows us to investigate the rapidity of climate shifts and centennial-scale change throughout the whole Holocene and late glacial in a way that was not possible with the previous, lower resolution records.

2 Site description

Nar Gölü (38°20'24''N, 34°27'23''E; 1363 m.a.s.l.; Figure 1) is a non-outlet, brackish maar lake, 0.7 km^2 in area and >20 m deep, in the Cappadocia region of central Turkey (see Dean et al., in press, for detailed catchment map). Modern $\delta^{18}O_{lakewater}$ values plot off the meteoric water line (average for July surface samples from the centre of the lake 2001-2012 was –1.3‰), suggesting high rates of evaporation (Jones et al., 2005; Dean et al., in press). The crater geology is dominated by basalt and ignimbrite (Gevrek and Kazancı, 2000), reducing the possibility for detrital carbonate contamination (cf. Leng et al., 2010). The climate of the region is continental Mediterranean (Kutiel and Türkeş, 2005). Annual precipitation at Niğde, 45 km from Nar Gölü, averaged 339 mm between 1935 and 2010. July, August and

September receive only 6% of the total precipitation, while April and May are the wettest months (27% of the total). The hottest months are July and August, when temperatures average +23°C, while from December to February temperatures average +0.7°C (meteorological data given in Dean et al., 2013).

Stable isotope (Jones et al., 2006; Dean et al., 2013), pollen (England et al., 2008) and diatom (Woodbridge and Roberts, 2011) studies have previously been carried out on a 1,720 year core sequence (NAR01/02) from the lake. The distinctive carbonate-organic couplets in the sediment have been shown to be annual (varves) and $\delta^{18}O_{carbonate}$ has been shown to provide a means of reconstructing water balance (Jones et al., 2005; Dean et al., in press).

Figure 1

3 Methods

3.1 Field work and chronology

Three parallel cores from the deepest part of Nar Gölü were retrieved using a UWITEC hammer-piston coring system, from the Laboratoire Environnement, Dynamiques et Territoires de la Montagne (EDYTEM), Université Savoie Mont Blanc, in July 2010. The three core sequences were matched visually at tie-points where turbidites or distinctive sedimentological patterns could be clearly correlated, which led to the compilation of a 21.7 m master sequence (NAR10).

Where possible, chronologies for the sequence were established by varve counting. Counts were made independently by two people and recounted until agreement (to within five varve years) was reached. However, as the core sequence was not varved throughout,

126 additional age estimates were needed. Radiocarbon dating had previously been undertaken on
127 bulk organic and carbonate samples known to be ~500 years old (dated by varve counting),
128 but these gave apparent radiocarbon ages of 14,320 and 23,450 years BP respectively,
129 indicating a substantial old carbon reservoir linked to volcanic out-gassing (Jones, 2004).
130 Pollen and charcoal could not be extracted in sufficient quantities for radiocarbon dating of
131 these components, and there were no terrestrial macrofossils found in the cores.
132 Uranium-thorium (U-Th) dating was carried out on two aragonite and four calcite
133 dominated horizons (Dean, 2014). The use of the U-Th system in lacustrine environments is
134 predicated on the assumption that carbonates incorporate soluble U from the water column,
135 but little Th, as the latter is insoluble and found in lower quantities in lake water (Edwards et
136 al., 2003). However, Th can be incorporated into carbonates at the time of deposition from
137 detrital material (detrital Th) and from the water column (hydrogenous Th), meaning initial
138 [$^{230}Th/^{234}U$] is often not zero, and corrections to single-sample ages and multi-sample
139 isochrons are required for accurate age determination (e.g. Hasse-Schram et al., 2004).
140 Samples were processed using a total dissolution approach following Bischoff and Fitzpatrick
141 (1991) and Luo and Ku (1991). Our analytical protocol was based on Edwards et al. (1987)
142 with modifications as described in Douarin et al. (2013). This protocol was further
143 augmented here to ensure complete silicate component dissolution. After initial dissolution of
144 the carbonate fraction from each sample using HNO_3 and isolation from the detritus by
145 centrifugation, the remaining insoluble silicate component was dissolved in a mixture of
146 HNO_3, HF and $HClO_4$ (all triple-distilled ultra-pure reagents) in an Evapoclean device to
147 ensure complete dissolution under clean lab conditions. The dissolved carbonate and detritus
148 fractions were then recombined and U and Th were separated and purified through anion
149 exchange chemistry. Samples were analysed on a Neptune Plus ICP-MS operating at c. 500-
150 600 V/ppm at an uptake rate of 50 µl/min through an Aridus II desolvating nebuliser. Data

reduction was achieved using an in-house Excel spreadsheet and the Isoplot 3 add-in (Ludwig, 2012) using the decay constants of Cheng et al. (2013). Isochrons were calculated following Ludwig and Titterington (1994) and Ludwig (2012).

3.2 Carbonate mineralogy

Different mineralogies of calcium carbonate fractionate oxygen isotopes differently (Sharp, 2007) such that it is important to establish the mineralogy of the carbonates prior to interpretation of carbonate isotope data (Leng and Marshall, 2004). Carbonate samples were prepared in cavity mounts as described by Hardy and Tucker (1998). The scanning range used on the X-ray Diffractometer (XRD; Siemens D500) was 5-65° 2θ and the scan rate was 2° 2θ per minute with a step size of 0.05. The TRACES program was used to identify which minerals were present. Where two or more carbonate minerals were present, the proportions of each were estimated by calculating the area under the XRD peaks and using experimentally calibrated conversion curves (Hardy and Tucker, 1988). Scanning Electron Microscopy (Philips XL30) and Energy-Dispersive X-ray Spectroscopy (EDS) (Oxford Instruments INCA) were used to provide images of carbonate crystals and to calculate elemental ratios.

3.3 Oxygen and carbon isotope analysis of carbonates

The XRD analyses showed that there are changes in carbonate mineralogy through the NAR10 core sequence, with calcite, aragonite and dolomite present at different times. This required samples for isotope analysis to be prepared in different ways.

175 Samples containing just calcite and/or aragonite were analysed for $\delta^{18}O$ and $\delta^{13}C$
176 using phosphoric acid, classic vacuum techniques, a standard +25.2°C reaction temperature
177 (McCrea, 1950; Craig, 1957) and a dual-inlet mass spectrometer. Data are given as ‰
178 deviations from VPDB and analytical reproducibility was 0.1‰ for $\delta^{18}O$ and $\delta^{13}C$. This
179 traditional reaction of carbonates at +25.2°C for 16 hours only partially reacts dolomite,
180 leading to an unpredictable kinetic fractionation. For samples composed of both dolomite and
181 aragonite/calcite, such as those in the Nar Gölü sequence, it is possible to extract CO_2 from
182 only the latter, without a significant reaction and accompanying fractionation of the dolomite,
183 by reducing the reaction time (Al-Aasm et al., 1990; Kyser et al., 2002; Baudrand et al.,
184 2012). We conducted experimental work to test whether a lower reaction temperature as well
185 as a shorter reaction time could be used to further limit the reaction of any dolomite within
186 the sample, and to test that this still led to the robust production of $\delta^{18}O$ data from calcite and
187 aragonite in these samples.
188 The experiments employed a calcite (KCM, marble) and dolomite standard (TDS,
189 hydrothermal dolomite) whose $\delta^{18}O$ values were –1.73‰ and –10.80‰ respectively. These
190 materials were chosen to mimic the calcite and dolomite at Nar Gölü. A range of mixtures of
191 the two standards were analysed and it was determined that for carbonate compositions with
192 <~20% dolomite, reaction at +16°C for 1 hour was sufficient to release enough CO_2 from the
193 calcite for analysis (using triple the amount of carbonate sample (i.e. ~30 mg in a carbonate-
194 rich sample) as would normally be used). Detrimental fractionation artefacts were not
195 observed and potential contributions of CO_2 from the dolomite were insignificant (Figure
196 A.1) based on the known isotope compositions of the starting materials. For most calcite-
197 dolomite mixtures containing >~20% dolomite, the offset from the accepted value of the
198 calcite component in the mixture was above expected analytical uncertainty and thus
199 interpreted to reflect a significant contribution from the dolomite (Figure A.1). Therefore,

samples containing >20% dolomite from the Nar Gölü core were not analysed for stable isotopes, and samples containing <20% were analysed following the reduced time and temperature reaction. The dolomite threshold adopted for Nar Gölü was very conservative to ensure that the analytical data interpreted here were an accurate representation, with a high degree of confidence, of the true calcite/aragonite isotope compositions. We acknowledge that the analytical reproducibility of the data from these dolomite-bearing samples may be greater than for those purely composed of calcite or aragonite, but given the large shifts seen in the Nar Gölü record any increased analytical uncertainties are dwarfed by the observed hydroclimate-induced changes to the isotopes. Our experiments are a promising first pass at defining appropriate analytical thresholds for dolomite-bearing lake carbonates and there is ample scope for further selective reaction method development to refine the analytical approach for lake sediment samples with significantly >20% dolomite.

4 Results

4.1 Lithology and chronology

There are two main lithologies in the NAR10 sequence: laminated sediments (alternating carbonate and organic layers, sometimes interrupted by turbidites) and non-laminated sediments (Figure 2). It is clear from modern monitoring studies (e.g. Dean et al., in press) and previous sediment core investigations (Jones et al., 2006; England et al., 2008; Woodbridge and Roberts, 2011) that laminations of late Holocene age are annual in origin (i.e. varved), and available evidence indicates that this is also true of most or all of the older laminations. In one section of the NAR10 cores (798-1038 cm), the laminations are often thicker (1-5 mm thick) suggesting the possibility of non-annual formation. However, because

U-Th dating is consistent with them being annual in origin (see below) we have assumed for the chronology presented here that these are varves as well. From 1038 to 1141 cm the laminations were often heavily deformed, making counting impossible. Mainly non-laminated sections are found at core depth intervals 598-754 cm, 1965-2053 cm and from 2133 cm to the base of the core.

Figure 2

The chronology is summarised in Figure 2 and U-Th data are given in Table A.1 and Figures A.2 and A.3.

Previous lake sediment studies (e.g. Hasse-Schramm et al., 2004) have shown that U-Th analysis of carbonates that have had their age constrained by other means, for example radiocarbon dating, provide critical constraints on the impact of potential hydrogenous Th. When present and unaccounted for, the hydrogenous Th component will result in U-Th ages that are older than the true age. Testing for the presence of hydrogenous Th was attempted by analysing the U-Th isotope compositions of carbonate-rich layers at 0ka and 1ka, as constrained by varve counting. The resulting U-Th data showed that the 0ka and 1ka carbonate layers unfortunately have high detritial Th content in addition to insufficient radiogenic ingrowth of ^{230}Th. No difference between the samples and typical continental detritus compositions could be determined (Figure A.2). As a result, the magnitude of any potential hydrogenous Th component at Nar Gölü remains indeterminate and therefore all of the isochron ages presented here best represent maximum ages for the dated horizons. Figure A.2 also shows that the turbidite samples from a layer ~6,500 years BP, considered here to be the most representative samples of end member detritus available and composed of silt- to

clay-sized silicates and no carbonate, overlap well within uncertainty of the average continental detritus composition.

U-Th analyses of carbonate-rich layers from various core depths were obtained to test for locations most favourable for more detailed sampling. These layers proved to be calcite-dominated, and although relatively carbonate-rich, they contained insufficiently high carbonate/detritus ratios and U/Th ratios to result in isotope compositions departing significantly from typical continental detritus compositions. Focus shifted to locating aragonite-rich layers that might provide higher U/Th ratios and a better contrast with the isotope composition of silicate detritus. Two horizons were thus identified, and the stratigraphically lower horizon, from 1949 cm depth, sampled to provide 5 subsamples of differing proportions of aragonite and detritus. U-Th analyses of these layers yielded a linear array with an age of 11.82 ± 0.52 ka (Table A.1, Figure A.3). Scatter in the data, indicated by a mean squared weighted deviation for the isochron regressed through the data points (MSWD) = 10.5, could indicate heterogeneity in the detrital component U and Th isotope composition. Following this analysis, the stratigraphically higher sample at 1021 cm was analysed. As relatively high clay content was noted, additional physical separation steps were taken to isolate the aragonite and coarse detritus components from the clay component, based on in-house experience gained with other ‘dirty’ carbonates (Sahy et al., 2014). Subsamples were sonicated in ultrapure water, and after a settling time of 1 hr the finest fraction remaining in suspension was isolated and discarded. This physical separation step resulted in a more favourable carbonate/detritus ratio composition, without risking disturbance of the U-Th systematics (cf. Bischoff and Fitzpatrick, 1991). An isochron age for this sample is 4.41 +0.16–0.17 ka (MSWD=1.7).

To aid comparison with previously published sequences, all varve counts and U-Th ages have been converted to years BP (i.e. before 1950) when plotted against age. It is

possible to use varve counting to provide a chronology for the sediments from the top of the sequence (AD2010) through to 2,557 years BP (598 cm). There is a gap in the varved sequence 598-754 cm but the 4.41 +0.16–0.17 ka U-Th age at 1021 cm ties the varved section of core between 754-1038 cm to an absolute chronology. Therefore, we were able to count up and down from this U-Th age to establish the chronology for this section. The chronology for the section 598-754 cm could then be determined by linear interpolation, assuming a fixed deposition rate for these largely homogenous sediments.

The 'floating' varved section of core 1161-1965 cm is tied by a U-Th age of 11.82 ±0.52 ka at 1949 cm. Below 1965 cm, there is a non-varved section of sediment, before a final floating varve sequence 2053-2133 cm. Again, we have assumed a linear deposition rate for the non-varved section 1965-2053 cm. We were not able to obtain a U-Th age constraint for the basal section of the core sequence, but the top of the basal varved section has been assigned an age of 12,900 years BP based on correlation with NGRIP (Rasmussen et al., 2006; Vinther et al., 2006). No data below 2133 cm are plotted against age.

The resulting age-depth model (Figure 2) indicates an overall sediment accumulation rate of 1.5 mm/yr^{-1} between ~12,000 and 2,000 years BP (~2000-500 cm depth), with an increase in mean sedimentation rate to ~2.5 mm/yr^{-1} in the last two millennia. Calculated sedimentation rates are lower during non-laminated core sections between 598 and 754 cm (dated 2,557-3,710 years BP) and 1965 to 2053 cm (dated 11,859-12,840 years BP), and are higher during the interval of thick laminations, 798-1038 cm (dated to 3,987-4,383 years BP). We estimated the sediments from 1141-1161 cm were lost during coring, but the sediments from before 1141 cm and after 1161 cm are radically different, which suggests there may also be a hiatus at this point in the NAR10 sequence. There are also deformed sediments 1038-1141 cm. Because of these problems, we have not included data 1038-1141 cm in the age model in this paper.

To check that the NAR01/02 and NAR10 sequences were overlapped at the correct tie-points and recorded the same isotope signature, $\delta^{18}O_{carbonate}$ data from the NAR10 record were compared to NAR01/02 data (Jones et al., 2006). The $\delta^{18}O_{carbonate}$ values from the matched stratigraphic points are very similar (mostly within analytical error), suggesting the $\delta^{18}O_{carbonate}$ values from the two core sequences are analogous, with age differences of <5 years at 1,400 years BP (Figure A.4). Counting of laminations from multiple replicate cores shows no evidence that deposition of turbidite layers led to varve removal, and hence to any under-estimate of true age.

4.2 Carbonate isotope and mineralogy data

Despite the changes in mineralogy, no correction has been made for the difference in the mineral-water fractionation factors of calcite and aragonite here because the difference is small ($\delta^{18}O$ of aragonite is ~0.7‰ more positive than $\delta^{18}O$ of calcite formed in the same $\delta^{18}O_{lakewater}$ and temperatures; Grossman and Ku, 1986; Kim et al., 2007) compared to the size of the shifts seen in this record. Additionally, calcite crystals from the NAR10 sequence were analysed by EDS and the average Ca/Mg ratio was 18.2 mol%, so Nar Gölü calcite is of a high-magnesium type (Gierlowski-Kordesch, 2010), and the offset in $\delta^{18}O$ between aragonite and high-magnesium calcite formed under the same conditions is even smaller than 0.7‰ (Tarutani et al., 1969; Jimenez-Lopez et al., 2004).

The period from the base of the core sequence up to ~2057 cm (Figure 3) has variable but generally lower $\delta^{18}O_{carbonate}$ (average –1.9‰) and $\delta^{13}C_{carbonate}$ (average +13.7‰) than the period from ~2053-1965 cm (average –0.6‰ and +18.8‰ respectively). Calcite/aragonite and varved sediments are found in the former whereas aragonite/dolomite and non-varved sediments are found in the latter. There is then a rapid shift to lower $\delta^{18}O_{carbonate}$ and

$\delta^{13}C_{carbonate}$ values and varved, calcite and aragonite sediments in the early Holocene (1957-1312 cm; average –2.9‰ and +13.4‰). $\delta^{18}O_{carbonate}$ values are fairly stable until increases to peaks (–1.0‰, –1.2‰ and 0.0‰) centred on ~1600, 1520 and 1450 cm respectively, all associated with shifts from calcite to aragonite. After ~1300 cm ($\delta^{18}O_{carbonate}$ –3.7‰), there is a sustained rise in $\delta^{18}O_{carbonate}$. The rise ends ~800 cm (+1.8‰) but high values are maintained, albeit with centennial-scale periods of lower $\delta^{18}O_{carbonate}$, until ~350 cm. $\delta^{13}C_{carbonate}$ values rise from +12.5‰ at ~1300 cm to >+17‰ ~800 cm. Dolomite is present from ~490-1050 cm, with the periods between ~920-1000, 600-680 and 540-580 cm having >20% dolomite, precluding $\delta^{18}O_{carbonate}$ analysis for the reasons outlined in section 3.3. At ~350 cm, there is a large transition to lower $\delta^{18}O_{carbonate}$ and $\delta^{13}C_{carbonate}$ and a shift from aragonite to calcite.

Figure 3

5 Discussion

5.1 Drivers of $\delta^{18}O_{carbonate}$ at Nar Gölü

A comparison of meteorological records to $\delta^{18}O_{lakewater}$ and $\delta^{18}O_{carbonate}$ data since 1999 (Dean et al., 2013; in press), and calibration with meteorological data (Jones et al., 2005), has shown $\delta^{18}O_{carbonate}$ from Nar Gölü is a strong proxy for regional water balance (with lower $\delta^{18}O_{carbonate}$ values when water balance was more positive, and vice versa). Several factors support the contention that water balance was the driver of $\delta^{18}O_{carbonate}$ throughout the NAR10 record.

Firstly, there is a strong co-variation between $\delta^{18}O_{carbonate}$ and $\delta^{13}C_{carbonate}$ (r=0.84, p=<0.001, n=1502, combining the NAR01/02 and NAR10 sequences; or r=0.83, n=465, p=<0.001 for just the NAR10 sequence) (Figures 3 and A.5). This can be taken to indicate that the lake has been hydrologically closed throughout this period (Talbot, 1990; Li and Ku, 1997). Lakes with no surface outflow such as Nar Gölü tend to have $\delta^{18}O$ records driven by changes in the evaporation:precipitation ratio (Leng and Marshall, 2004).

Secondly, varves are only preserved in lakes when water depth is sufficient to limit turbidity caused by wind and when there is stratification leading to anoxic bottom waters and consequent limited bioturbidity (Ojala et al., 2000; Ojala et al., 2012; Zolitschka et al., 2015). A shift from varved to non-varved lake sediments is therefore likely to reflect a shift to lower lake levels. The observation that varved sediments occur when $\delta^{18}O_{carbonate}$ is lowest, and non-varved when $\delta^{18}O_{carbonate}$ is highest, supports the interpretation of $\delta^{18}O_{carbonate}$ as a water balance proxy.

Thirdly, shifts from calcite to aragonite are believed to occur due to an increase in the Mg/Ca ratio of lake water (Müller et al., 1972; Kelts and Hsu, 1978; Ito, 2001), which favours the precipitation of aragonite over calcite (Berner, 1975; De Choudens-Sanchez and Gonzalez, 2009). This shift has been observed in Nar Gölü over the last decade, as the lake level has fallen and Mg/Ca ratios have increased (Dean et al., in press). Dolomite is found in parts of the sequence, but unlike calcite and aragonite there is no evidence for dolomite forming during our monitoring period (1997-present). Dolomite in lake sediments can originate from the detrital inwash of old dolomite, from primary precipitation, or from diagenetic precipitation in sediments (Armenteros, 2010; Leng et al., 2010). At Nar Gölü, the former can be discounted as the crater geology is dominated by basalt and ignimbrite. Primary dolomites are rare in lake sediments, however where they do occur they tend to have rhombic crystals (Sabins, 1962) whilst those in Nar Gölü sediments are subhedral/anhedral

(Figure A.6). It is possible that dolomite formed authigenically within the sediments, replacing calcite or aragonite during early diagenesis. An organogenic origin is plausible, given the dolomite is calcium-rich (average Ca/Mg ratio of dolomite crystals is 2.3) (Vasconcelos and McKenzie, 1997; Armenteros, 2010) and due to the porous nature of the crystals (Figure A.6; Deng et al., 2010). Regardless of the actual mode of formation, it is widely accepted that dolomite formation requires sufficient magnesium (Mazzullo, 2000), so the appearance of dolomite in the sediments suggests magnesium was more highly concentrated than at times when aragonite or calcite formed. Dolomite was also precipitated at similar times in the late Holocene at another maar lake in the same region (Eski Acıgöl; Roberts et al., 2001), implying a common origin linked to low lake levels and dry climatic conditions. $\delta^{18}O_{carbonate}$ values are highest when dolomite is present, lower in aragonite zones and lowest in calcite zones, again showing that $\delta^{18}O$ values follow evaporation trends.

5.2 Hydroclimate reconstructions

5.2.1 The late glacial

Full chronological control below 1965 cm is lacking. However, the low $\delta^{18}O_{carbonate}$ values and varved sediments from 2053 cm to the bottom of the core sequence indicate a wetter period probably at the time of the Bølling-Allerød and the higher $\delta^{18}O_{carbonate}$ values, aragonite/dolomite and non-varved sediments 1965-2053 cm (Figure 3) indicate a dry period at the time of the Younger Dryas. This would follow the pattern of late glacial hydroclimate previously reconstructed in the region (e.g. Jones et al., 2007; Kotthoff et al., 2008; Wilson et al., 2008).

The magnitude of change in $\delta^{18}O$ during the entire transition from the Younger Dryas-aged dry period into the Holocene is 5.2‰ (Figure 4). Because of the chronological uncertainty, it is not possible to calculate precisely how long the entire transition took, but based on deposition rates of adjacent sections we can estimate it took <200 years. Over half of the $\delta^{18}O_{carbonate}$ transition (2.9‰) occurs in just 9 varve years (Figure 4), although after this shift there is a change back to higher $\delta^{18}O_{carbonate}$ values, in an excursion that lasts 27 varve years, before a return to lower $\delta^{18}O_{carbonate}$. The nature of the transition recorded by $\delta^{18}O_{carbonate}$ could indicate a non-linear response of $\delta^{18}O_{carbonate}$ to changing climate and/or that the climate transition itself was non-linear.

Figure 4

5.2.2 General Holocene trends

The Nar Gölü $\delta^{18}O_{carbonate}$ record is similar to other lake $\delta^{18}O$ records from the Eastern Mediterranean (Figure 5) (Roberts et al., 2008; 2011). Specifically, there are low $\delta^{18}O_{carbonate}$ values at Nar Gölü in the early Holocene and a clear and sustained transition to higher values (albeit interrupted by centennial-scale fluctuations) that starts ~7,600 years BP and ends ~4,000 years BP (Figure 5). This period of high $\delta^{18}O_{carbonate}$ at Nar Gölü lasts until ~1,500 years BP. These timings are similar to other records from the region (Roberts et al., 2011). There are shifts from calcite prior to ~6,500 years BP to aragonite and dolomite for most of the later Holocene, from varved to at times non-varved sediments and from low to high $\delta^{13}C_{carbonate}$. This supports the interpretation of Holocene $\delta^{18}O_{carbonate}$ in Eastern Mediterranean lake carbonates as responding to water balance (Jones and Roberts, 2008), rather than to changes in the $\delta^{18}O$ of the source of precipitation (Litt et al., 2012) or in the

seasonality of precipitation (Stevens et al., 2001; 2006), since changes in carbonate mineralogy, lithology and $\delta^{13}C_{carbonate}$ can be influenced by changes in water balance but not directly by the other two factors (Leng and Marshall, 2004).

Figure 5

5.2.3 Centennial-scale 'events' in the early Holocene

Two main periods of centennial-scale climate change in the early Holocene have been identified from North Atlantic region palaeoclimate records: the so-called 9.3ka and 8.2ka 'events' (Rasmussen et al., 2006). Climate changes at the time of the 8.2ka 'event' have been identified in some Eastern Mediterranean records (Bar-Matthews et al., 2003; Landmann and Kempe, 2005; Turner et al., 2008), however a lack of high-resolution records means investigation of other centennial-scale changes in the early Holocene has been limited. The uncertainties on the U-Th date at 1949 cm mean it is not possible to investigate fully whether the early Holocene events occurred synchronously in Nar Gölü and NGRIP. However, it is possible to count through the varved sediments from the start of the Holocene to establish whether there were any changes in Nar Gölü that occurred the same amount of time from the start of the Holocene in central Turkey as equivalent changes after the onset of the Holocene in Greenland. We define the durations of the events simply by eye, following the logic of Daley et al. (2011) that statistical approaches may not be suitable when comparing such diverse data sets.

There is a shift to increasing dryness in Nar Gölü ~2,340 varve years after the start of the Holocene, very similar to the number of years after the start of the Holocene the 9.3ka cooling trend starts in NGRIP (Figure 6). However, whereas the cooling in NGRIP and other

447 records from the North Atlantic region such as Ammersee (von Grafenstein et al., 1999) lasts
448 ~100 years, in Nar Gölü the excursion lasts ~300 years (Figure 6). Relative dryness at this
449 time also lasts longer in other records more remote from the North Atlantic, for example
450 Dongge in China, where the excursion lasts ~200 years (Dykoski et al., 2005).

451 There is a peak in $\delta^{18}O_{carbonate}$ in Nar Gölü starting ~3,400 years after the start of the
452 Holocene, around the time of the 8.2ka 'event' in NGRIP. However, this appears to be the
453 peak of a longer isotope trend encompassing ~300 years (Figure 6). There is also a switch
454 from calcite to aragonite sediments for ~400 years at the time of the highest isotope values.
455 The 8.2ka 'event' is seen across the Northern Hemisphere (Alley et al., 1997; Alley and
456 Ágústsdóttir, 2005; Morrill and Jacobsen, 2005). In NGRIP it is defined as lasting 160 years
457 (Thomas et al., 2007), and in other isotope records from the North Atlantic region ~150±30
458 years (Daley et al., 2011). However, other than in a few records (e.g. Heshang Cave in China;
459 Liu et al., 2013), away from the North Atlantic region the effects are often spread over a
460 longer time period (Rohling and Pälike, 2005; Wiersma and Renssen, 2006; Thomas et al.,
461 2007), with more abrupt changes at 8,200 years BP superimposed on longer term
462 cooling/drying trends (Rohling and Pälike, 2005). Intervals where the climate became drier
463 compared to average early Holocene conditions are seen in records from across tropical
464 Africa ~8,500-7,800 years BP (Gasse, 2000), the Black Sea coast of Turkey ~8,400-7,800
465 years BP (Göktürk et al., 2011) and for several hundred years in Qunf Cave in Oman
466 (Fleitmann et al., 2003; 2007) (Figure 6). A dry event in between those centred on ~9,300 and
467 8,200 years BP is seen in both Nar Gölü and Qunf, as are shifts to lower $\delta^{18}O_{carbonate}$ either
468 side of this dry event (Figure 6).
469
470 Figure 6
471

5.2.4 Centennial-scale 'events' in the mid to late Holocene

Over 2,000 years of data are either missing from the core sequence or are not shown on Figure 5 because of uncertainties in the chronology (section 4.1). Therefore, it is not possible to investigate whether a drought previously identified in the region ~5,300-5,000 years BP (Bar-Matthews and Ayalon, 2011; Kuzucuoğlu et al., 2011) occurred at Nar Gölü.

It is possible, however, to investigate changes from 4,400 years BP to the present day. Firstly, there was >20% dolomite content ~4,300-4,150 years BP, indicating a period of very negative water balance (i.e. dry conditions). Following this, once dolomite levels fell below 20%, the highest $\delta^{18}O_{carbonate}$ values in the whole sequence occurred at ~3,800 years BP. Previous studies have identified substantial drying ~4,200-3,900 years BP in the Eastern Mediterranean (Cullen et al., 2000; Eastwood et al., 2007; Ulgen et al., 2012). This dry interval has been called the 4.2ka 'event' and coincides with the decline of the Akkadian Empire in northern Mesopotamia (Weiss, 1993; Cullen et al., 2000) and the Old Kingdom of Egypt (Stanley et al., 2003).

There is a further positive $\delta^{18}O_{carbonate}$ excursion in Nar Gölü ~3,400 years BP, coincident with a period of dryness identified in Eski Acıgöl and Van (Roberts et al., 2011) (Figure 5). There are two periods of high (>20%) dolomite ~3,150-2,550 and ~2,500-2,300 years BP. These again suggest drier conditions than the millennial-average, and the presence of non-varved sediments for the first of these periods could be taken to indicate an even drier climate than in the interval ~4,300-4,150 years BP. The period ~3,150-2,550 years BP is synchronous within dating uncertainty with a drought seen across the Eastern Mediterranean (Roberts et al., 2001; Verheyden et al., 2008; Langgut et al., 2013; Neugebauer et al., 2015), at the time of the so-called Late Bronze Age Collapse/Crisis (Kaniewski et al., 2013) when civilisations such as the Hittites in central Turkey went into decline (Weiss, 1982; Akurgal,

2001). The period ~2,500-2,300 years BP could be coincident with some peaks seen in the Eski Acıgöl $\delta^{18}O_{carbonate}$ record, but more high-resolution records from the region are required to help establish if there was a widespread excursion to increasing dryness at this time.

5.2.5 The large shift in $\delta^{18}O_{carbonate}$ in the 6th century AD

There is a large shift to more negative $\delta^{18}O_{carbonate}$ in the 6th century AD: ~1,450-1,400 years BP (Figures 5 and A.4). This period of low $\delta^{18}O_{carbonate}$ lasted until ~550 years BP, interrupted by a temporary rise to higher values ~1,090 years BP. Other than the multi-millennial scale Mid Holocene Transition, it is the largest $\delta^{18}O$ shift seen in the record, even more pronounced than the late glacial to Holocene transition. Around the Eastern Mediterranean, a shift to wetter conditions is inferred at this time in Soreq Cave (Orland et al., 2009), Lake Tecer (Kuzucuoğlu et al., 2011), the Eastern Mediterranean Sea (Schilman et al., 2001) and the Dead Sea (Neumann et al., 2007). However, only at Nar Gölü is the shift of such a high magnitude. As well as the shift to lower $\delta^{18}O_{carbonate}$, indicative of a shift to more positive water balance, the shift from aragonite to calcite precipitation, and diatom assemblage data (Woodbridge and Roberts, 2011), also indicate a shift to wetter conditions.

5.3 Drivers of Eastern Mediterranean hydroclimate

The rapidity of the late glacial to Holocene transition at Nar Gölü is comparable to that seen in temperature records from the North Atlantic region (e.g. von Grafenstein et al., 1999; Rasmussen et al., 2006). This suggests a strong teleconnection between the North Atlantic and Eastern Mediterranean. A rapid transition into the Holocene is also seen in Moomi Cave in Socotra, Yemen (Shakun et al., 2007), and in Hulu and Kulishu caves in

China (Wang et al., 2001; Ma et al., 2012; Orland et al., in press) (see Figure 1 for locations). The transition is more gradual in Dongge; differences between the Chinese speleothem records could be related to differences in the relative influences of the Indian Monsoon and the East Asian Monsoon, and westerlies, at different sites (Huang et al., 2015).

On the whole, central Turkey was drier when the North Atlantic was cooler: at the time of the Younger Dryas, at ~9,300 years BP, ~8,200 years BP, ~4,200 years BP and ~3,100 years BP. Slowdowns of North Atlantic thermohaline circulation due to glacial outburst floods have been suggested as the causes of the Younger Dryas (Teller, 2012), 9.3ka (Fleitmann et al., 2008; Yu et al., 2010) and 8.2ka (Thomas et al., 2007; Hoogakker et al., 2011; Hoffman et al., 2012) cooling episodes. Although there is no clear climate signal in the NGRIP ice core ~4,200 and 3,100 years BP, increases in ice-rafted debris in the North Atlantic known as Bond events 3 and 2 (Bond et al., 1997) occur around these times. A significant amount of the precipitation that falls in central Turkey has North Atlantic origins (Harding et al., 2009; Türkeş et al., 2009) so a reduction in cyclogenesis at these cooler times is likely to have reduced the frequency, and potentially changed the path, of storm tracks from the Atlantic. A resulting reduction in Mediterranean cyclogenesis is also likely. Together, this would have led to less precipitation in the Eastern Mediterranean (Bartov et al., 2003; Prasad et al., 2004; Rowe et al., 2012).

The influence of the North Atlantic through ocean and/or atmospheric circulation could explain peaks in dryness at Nar Gölü at these times, but does not explain why the excursions ~9,300 and 8,200 years BP last longer in Nar Gölü and other records outside of the North Atlantic region (Rohling and Pälike, 2005) than the cooling 'events' in the North Atlantic. Whilst changes in the North Atlantic are seen as a key driver of Eastern Mediterranean hydroclimate in the present and past, it has been demonstrated that other teleconnections are also important, such as Indian Summer Monsoon dynamics (Jones et al.,

2006; Ziv et al., 2006) and the North Sea-Caspian Pattern Index (Kutiel and Türkeş, 2005). Jones et al. (2006) used the 1,720-year NAR01/02 record to show changes in the North Atlantic have more of an influence on winter conditions and changes in the Indian Summer Monsoon have more of an influence on summer conditions at Nar Gölü. Rohling and Pälike (2005) suggest the sharp 8.2ka event signal is seen more in winter-based proxies with the broader ~8,500-8,000 years BP climate deterioration more evident in summer-weighted proxies. There seem to be drier summers at Nar Gölü over the past 1,720 years when the monsoon is more intense (Jones et al., 2006), hypothesised to be related to a strengthening of the descending branch of the Hadley cell and increased northerly winds over the Eastern Mediterranean at these times (Raicich et al., 2003; Tyrlis et al., 2013). However, ~8,200 years BP, we see a different relationship, with seemingly concomitant shifts at Nar Gölü and Qunf to drier conditions, related, at least in the latter case, to a less intense monsoon (Fleitmann et al., 2003). Reduced solar output has been proposed as the cause of the broad underlying climate deterioration ~8,500-8,000 years BP (Neff et al., 2001; Gupta et al., 2005; Rohling and Pälike, 2005). This could explain a weakening of the monsoon, but it remains unclear how reduced energy in the climate system would lead to increased evaporation in the summer at Nar Gölü. Reduced summer precipitation would give a similar signal, to more positive isotope values, but many authors suggest that summers had low precipitation throughout the early Holocene, with significant rainfall only falling in the winter (see discussion below). Whatever the cause, changes in the North Atlantic ~8,200 years BP additionally led to drier winters (less precipitation) and even higher $\delta^{18}O_{carbonate}$ at Nar Gölü, accounting for the maxima of the peak at Nar Gölü at this time.

There is a large, multi-millennial scale shift in Holocene hydroclimate seen in Nar Gölü and other records from the Eastern Mediterranean (e.g. Roberts et al., 2001; Eastwood et al., 2007), Asia (e.g. Fleitmann et al., 2003; Dykoski et al., 2005) and Africa (e.g. Adkins

et al., 2006; Renssen et al., 2006): the Mid Holocene Transition. This suggests that there are additional drivers of Eastern Mediterranean hydroclimate, in this case at millennial-scales. The Mid Holocene Transition has been linked to a decline in Northern Hemisphere summer insolation from the early Holocene maximum (deMenocal et al., 2000; Braconnot et al., 2007; Fleitmann et al., 2007; Renssen et al., 2007). Increased precipitation in Saharan Africa in the early Holocene was caused by a northward movement of the Inter Tropical Convergence Zone and monsoon rains related to this peak in insolation (Schneider et al., 2014), but the direct influence of the African Monsoon is not generally considered to have reached the Eastern Mediterranean (Arz et al., 2003; Brayshaw et al., 2011a). Summer drought persisted for several millennia into the Holocene in the Eastern Mediterranean (Turner et al., 2010; Peyron et al., 2011; Vanniere et al., 2011). Rather, the wet early Holocene in the Eastern Mediterranean appears to have been the result of increased precipitation in other seasons, especially the winter (Brayshaw et al., 2011b), made possible because of the increased residual heat left in the North Atlantic and the Mediterranean Sea as a result of the higher summer insolation (Tzedakis, 2007), increasing cyclogenesis. Through the Holocene, a decrease in annual insolation led to a weakening and poleward shift of the storm track (Black et al., 2011), and to drier conditions in the Eastern Mediterranean.

6 Conclusion

Using $\delta^{18}O_{carbonate}$ and carbonate mineralogy data, on a core sequence dated by U-Th and varve counting, it has been possible to provide a highly-resolved hydroclimatic reconstruction for the Eastern Mediterranean. We show relatively dry conditions at the time of the Younger Dryas, a wet early Holocene and the Mid Holocene Transition to drier conditions, which peaked ~4,200-1,500 years BP. There are centennial-scale periods where

climate became drier than the millennial average ~9,300, 8,200, 4,200 and 3,100 years BP. Other studies have previously suggested a link between Eastern Mediterranean hydroclimate and changes in the North Atlantic during the last glacial (e.g. Bartov et al., 2003) and late Holocene (e.g. Jones et al., 2006), but it is only with the high-resolution record presented here that we can demonstrate this was the case in the early Holocene as well. We show that dry climatic anomalies during the late glacial and throughout the Holocene in central Turkey appear to occur at the same time as cold anomalies in the North Atlantic. This suggests a teleconnection between the two regions, via changes in cyclogenesis and in the frequency and path of storm tracks from the Atlantic. However, the Mid Holocene Transition and the longer duration of the 9.3ka and 8.2ka anomalies at Nar Gölü indicate there are additional controls on Eastern Mediterranean hydroclimate.

Acknowledgments

JRD was funded by NERC PhD studentship NE/I528477/1 (2010-2014). Isotope and U-Th work was funded by NIGFSC grants IP/1198/1110 and IP/1237/0511 to MDJ. Fieldwork was supported by National Geographic and British Institute at Ankara grants to CNR. MJL oversaw the stable isotope work and assisted JRD, MDJ and SEM with the interpretation of these data, and HJS developed the selective reaction method for samples containing both calcite and dolomite. SRN and DS led the U-Th work. JRD, MDJ, CNR, WJE and SEM assessed the implications for regional palaeoclimatology. All authors have contributed intellectually to the manuscript and have approved the final version. We would like to thank those others who contributed to fieldwork in 2010 at Nar Gölü: Hakan Yiğitbaşıoğlu, Fabien Arnaud, Emmanuel Malet, Ersin Ateş, Çetin Şenkul, Gwyn Jones, Ryan Smith and Ceran Şekeryapan, as well as the British Institute at Ankara for logistical support. Christopher

Kendrick, Ewan Woodley, Jonathan Lewis, Carol Arrowsmith, Graham Morris, Teresa Needham and David Clift all provided laboratory support. We are especially thankful to Samantha Allcock for help in the field and with the varve counts. The underlying data can be found in the online materials. Finally, we thank two anonymous reviewers for their thorough comments that improved the original manuscript. This work is published with the permission of the Executive Director of the British Geological Survey.

References

Adkins, J., DeMenocal, P., Eshel, G., 2006. The "African humid period" and the record of marine upwelling from excess Th-230 in Ocean Drilling Program Hole 658C. Paleoceanography 21, PA4203.

Akurgal, E., 2001. The Hattian and Hittite Civilizations. Ministry of Culture, Ankara.

Al-Aasm, I.S., Taylor, B.E., South, B., 1990. Stable isotope analysis of multiple carbonate samples using selective acid-extraction. Chem Geol 80, 119-125.

Alley, R.B., Ágústsdóttir, A.M., 2005. The 8k event: cause and consequences of a major Holocene abrupt climate change. Quat Sci Rev 24, 1123-1149.

Alley, R.B., Mayewski, P.A., Sowers, T., Stuiver, M., Taylor, K.C., Clark, P.U., 1997. Holocene climatic instability: a prominent, widespread event 8200 yr ago. Geology 25, 483-486.

Almogi-Labin, A., Bar-Matthews, M., Shriki, D., Kolosovsky, E., Paterne, M., Schilman, B., Ayalon, A., Aizenshtat, Z., Matthews, A., 2009. Climatic variability during the last ~90 ka of the southern and northern Levantine Basin as evident from marine records and speleothems. Quat Sci Rev 28, 2882-2896.

646 Armenteros, I., 2010. Diaganesis of Carbonates in Continental Settings, in: Alonso-Zara,
647 A.M., Tanner, L.H. (Eds.), Developments in Sedimentology vol. 62. Geochemistry,
648 Diagenesis and Applications. Elsevier, Amsterdam, pp. 61-152.
649 Arz, H.W., Lamy, F., Patzold, J., Muller, P.J., Prins, M., 2003. Mediterranean moisture
650 source for an early-Holocene humid period in the northern Red Sea. Science 300, 118-
651 121.
652 Bar-Matthews, M., Ayalon, A., Kaufman, A., 1997. Late Quaternary paleoclimate in the
653 eastern Mediterranean region from stable isotope analysis of speleothems at Soreq
654 Cave, Israel. Quat Res 47, 155-168.
655 Bar-Matthews, M., Ayalon, A., Kaufman, A., Wasserburg, G.J., 1999. The Eastern
656 Mediterranean paleoclimate as a reflection of regional events: Soreq cave, Israel. Earth
657 Planet Sc Lett 166, 85-95.
658 Bar-Matthews, M., Ayalon, A., 2011. Mid-Holocene climate variations revealed by high-
659 resolution speleothem records from Soreq Cave, Israel and their correlation with
660 cultural changes. Holocene 21, 163-171.
661 Bar-Matthews, M., Ayalon, A., Gilmour, M., Matthews, A., Hawkesworth, C.J., 2003. Sea-
662 land oxygen isotopic relationships from planktonic foraminifera and speleothems in the
663 Eastern Mediterranean region and their implication for paleorainfall during interglacial
664 intervals. Geochim Cosmochim Acta 67, 3181-3199.
665 Bartov, Y., Goldstein, S.L., Stein, M., Enzel, Y., 2003. Catastrophic arid episodes in the
666 Eastern Mediterranean linked with the North Atlantic Heinrich events. Geology 31,
667 439-442.
668 Baudrand, M., Aloisi, G., Lecuyer, C., Martineau, F., Fourel, F., Escarguel, G., Blanc-
669 Valleron, M.M., Rouchy, J.M., Grossi, V., 2012. Semi-automatic determination of the

carbon and oxygen stable isotope compositions of calcite and dolomite in natural mixtures. Appl Geochem 27, 257-265.

Berner, R.A., 1975. The role of magnesium in the crystal growth of calcite and aragonite from sea water. Geochim Cosmochim Acta 39, 489-504.

Bischoff, J.L., Fitzpatrick, J.A., 1991. U-Series dating of impure carbonates - an isochron technique using total-sample dissolution. Geochim Cosmochim Acta 55, 543-554.

Black, E., Brayshaw, D., Black, S., Rambeau, C., 2011. Using Proxy Data, Historical Climate Data and Climate Models to Investigate Aridification During the Holocene, in: Mithen, S., Black, E. (Eds.), Water, Life and Civilisation. Cambridge University Press, Cambridge, pp. 105-112.

Bond, G., Showers, W., Cheseby, M., Lotti, R., Almasi, P., DeMenocal, P., Priore, P., Cullen, H., Hajdas, I., Bonani, G., 1997. A pervasive millennial-scale cycle in North Atlantic Holocene and glacial climates. Science 278, 1257-1266.

Braconnot, P., Otto-Bliesner, B., Harrison, S., Joussaume, S., Peterchmitt, J.Y., Abe-Ouchi, A., Crucifix, M., Driesschaert, E., Fichefet, T., Hewitt, C.D., Kageyama, M., Kitoh, A., Loutre, M.F., Marti, O., Merkel, U., Ramstein, G., Valdes, P., Weber, L., Yu, Y., Zhao, Y., 2007. Results of PMIP2 coupled simulations of the Mid-Holocene and Last Glacial Maximum - Part 2: feedbacks with emphasis on the location of the ITCZ and mid- and high latitudes heat budget. Clim Past 3, 279-296.

Brayshaw, D., Black, E., Hoskins, B., Slingo, J., 2011a. Past Climates of the Middle East, in: Mithen, S., Black, E. (Eds.), Water, Life and Civilisation. Cambridge University Press, Cambridge, pp. 25-50.

Brayshaw, D.J., Rambeau, C.M.C., Smith, S.J., 2011b. Changes in Mediterranean climate during the Holocene: insights from global and regional climate modelling. Holocene 21, 15-31.

Castañeda, I.S., Schefuss, E., Patzold, J., Damste, J.S.S., Weldeab, S., Schouten, S., 2010. Millennial-scale sea surface temperature changes in the eastern Mediterranean (Nile River Delta region) over the last 27,000 years. Paleoceanography 25, PA1208.

Cheng, H., Edwards, R.L., Shen, C., Polyak, V.J., Asmerom, Y., Woodhead, J., Hellstrom, J., Wang, Y., Kong, X., Spötl, C., Wang, X., Alexander, E. J., 2013. Improvements in ^{230}Th dating, ^{230}Th and ^{234}U half-life values, and U–Th isotopic measurements by multi-collector inductively coupled plasma mass spectrometry. Earth Planet Sc Lett 371, 82-91.

Craig, H., 1957. Isotopic standards for carbon and oxygen and correction factors for mass-spectrometric analysis of carbon dioxide. Geochim Cosmochim Acta 12, 133-149.

Cullen, H.M, deMenocal, P.B., 2000. North Atlantic influence on Tigris-Euphrates streamflow. Int J Climatol 20, 853-863.

Cullen, H.M., deMenocal, P.B., Hemming, S., Hemming, G., Brown, F.H., Guilderson, T., Sirocko, F., 2000. Climate change and the collapse of the Akkadian empire: evidence from the deep sea. Geology 28, 379-382.

Daley, T.J., Thomas, E.R., Holmes, J.A., Street-Perrott, F.A., Chapman, M.R., Tindall, J.C., Valdes, P.J., Loader, N.J., Marshall, J.D., Wolff, E.W., Hopley, P.J., Atkinson, T., Barber, K.E., Fisher, E.H., Robertson, I., Hughes, P.D.M., Roberts, C.N., 2011. The 8200 yr BP cold event in stable isotope records from the North Atlantic region. Glob Planet Chang 79, 288-302.

Dean, J.R., 2014. Stable Isotope Analysis and U-Th dating of Late Glacial and Holocene Lacustrine Sediments from Central Turkey. PhD, Nottingham.

Dean, J.R., Jones, M.D., Leng, M.J., Sloane, H.J., Roberts, C.N., Woodbridge, J., Swann, G.E.A., Metcalfe, S.E., Eastwood, W.J., Yigitbasioglu, H., 2013. Palaeo-seasonality of

719 the last two millennia reconstructed from the oxygen isotope composition of carbonates
720 and diatom silica from Nar Gölü, central Turkey. Quat Sci Rev 66, 35-44.
721 Dean, J.R., Eastwood, W.J., Roberts, C.N., Jones, M.D., Yiğitbaşıoğlu, H., Allcock, S.L.,
722 Woodbridge, J., Metcalfe, S.E., Leng, M.J., In press. Tracking the hydro-climatic signal
723 from lake to sediment: a field study from central Turkey. J Hydrol.
724 http://www.dx.doi.org/10.1016/j.jhydrol.2014.11.004
725 De Choudens-Sanchez, V., Gonzalez, L.A., 2009. Calcite and aragonite precipitation under
726 controlled instantaneous supersaturation: elucidating the role of Caco(3) saturation state
727 and Mg/Ca Ratio on calcium carbonate polymorphism. J Sediment Res 79, 363-376.
728 deMenocal, P., Ortiz, J., Guilderson, T., Adkins, J., Sarnthein, M., Baker, L., Yarusinsky, M.,
729 2000. Abrupt onset and termination of the African Humid Period: rapid climate
730 responses to gradual insolation forcing. Quat Sci Rev 19, 347-361.
731 Deng, S.C., Dong, H.L., Lv, G., Jiang, H.C., Yu, B.S., Bishop, M.E., 2010. Microbial
732 dolomite precipitation using sulfate reducing and halophilic bacteria: results from
733 Qinghai Lake, Tibetan Plateau, NW China. Chem Geol 278, 151-159.
734 Douarin, M., Elliot, M., Noble, S.R., Sinclair, D., Henry, L.-A., Long, D., Moreton, S.G.,
735 Roberts, J.M., 2013. Growth of north-east Atlantic cold-water coral reefs and mounds
736 during the Holocene: A high resolution U-series and ^{14}C chronology. Earth Planet Sc
737 Lett 375, 176-187.
738 Dykoski, C.A., Edwards, R.L., Cheng, H., Yuan, D.X., Cai, Y.J., Zhang, M.L., Lin, Y.S.,
739 Qing, J.M., An, Z.S., Revenaugh, J., 2005. A high-resolution, absolute-dated Holocene
740 and deglacial Asian monsoon record from Dongge Cave, China. Earth Planet Sc Lett
741 233, 71-86.

742 Eastwood, W.J., Leng, M.J., Roberts, N., Davis, B., 2007. Holocene climate change in the
743 eastern Mediterranean region: a comparison of stable isotope and pollen data from Lake
744 Golhisar, southwest Turkey. J Quat Sci 22, 327-341.
745 Edwards, R.L., Chen, J.H., Wasserburg, G.J., 1987. ^{238}U, ^{234}U, ^{230}Th, ^{232}Th systematics and
746 the precise measurement of time over the past 500,000 years. Earth Planet Sc Lett 81,
747 175-192.
748 Edwards, R.L., Gallup, C.D., Cheng, H., 2003. Uranium-series dating of marine and
749 lacustrine carbonates. Rev Mineral Geochem 52, 363-40.
750 England, A., Eastwood, W.J., Roberts, C.N., Turner, R., Haldon, J.F., 2008. Historical
751 landscape change in Cappadocia (central Turkey): a palaeoecological investigation of
752 annually laminated sediments from Nar lake. Holocene 18**,** 1229-1245.
753 Fleitmann, D., Burns, S.J., Mangini, A., Mudelsee, M., Kramers, J., Villa, I., Neff, U., Al-
754 Subbary, A.A., Buettner, A., Hippler, D., Matter, A., 2007. Holocene ITCZ and Indian
755 monsoon dynamics recorded in stalagmites from Oman and Yemen (Socotra). Quat Sci
756 Rev 26, 170-188.
757 Fleitmann, D., Burns, S.J., Mudelsee, M., Neff, U., Kramers, J., Mangini, A., Matter, A.,
758 2003. Holocene forcing of the Indian monsoon recorded in a stalagmite from Southern
759 Oman. Science 300, 1737-1739.
760 Fleitmann, D., Mudelsee, M., Burns, S.J., Bradley, R.S., Kramers, J., Matter, A., 2008.
761 Evidence for a widespread climatic anomaly at around 9.2 ka before present.
762 Paleoceanography 23, PA1102.
763 Gasse, F., 2000. Hydrological changes in the African tropics since the Last Glacial
764 Maximum. Quat Sci Rev 19, 189-211.

765 Gevrek, A.I., Kazanci, N., 2000. A Pleistocene, pyroclastic-poor maar from central Anatolia,
766 Turkey: influence of a local fault on a phreatomagmatic eruption. J Volcanol Geoth Res
767 95, 309-317.
768 Gierlowski-Kordesch, E., 2010. Lacustrine Carbonates, in: Alonso-Zara, A.M., Tanner, L.H.
769 (Eds.), Carbonates in Continental Settings: Facies, Environments and Processes.
770 Elsevier, Amsterdam, pp. 1-102.
771 Göktürk, O.M., Fleitmann, D., Badertscher, S., Cheng, H., Edwards, R.L., Leuenberger, M.,
772 Fankhauser, A., Tuysuz, O., Kramers, J., 2011. Climate on the southern Black Sea coast
773 during the Holocene: implications from the Sofular Cave record. Quat Sci Rev 30,
774 2433-2445.
775 Grossman, E.L., Ku, T.L., 1986. Oxygen and carbon isotope fractionation in biogenic
776 aragonite - temperature effects. Chem Geol 59, 59-74.
777 Gupta, A.K., Das, M., Anderson, D.M., 2005. Solar influence on the Indian summer monsoon
778 during the Holocene. Geophys Res Lett 32, L17703.
779 Harding, A., Palutikof, J., Holt, T., 2009. The Climate System, in: Woodward, J. (Ed.), The
780 Physical Geography of the Mediterranean. Oxford University Press, Oxford, pp. 69–88.
781 Hardy, R., Tucker, M., 1988. X-ray Powder Diffraction of Sediments, in: Tucker, M. (Ed.),
782 Techniques in Sedimentology. Blackwell, Oxford.
783 Hasse-Schramm, A., Goldstein, S.L., Stein, M., 2004. U-Th dating of Lake Lisan (late
784 Pleistocene Dead Sea) aragonite and implications for glacial East Mediterranean
785 climate change. Geochim Cosmochim Acta 68, 985-1005.
786 Hoffman, J.S., Carlson, A.E., Winsor, K., Klinkhammer, G.P., LeGrande, A.N., Andrews,
787 J.T., Strasser, J.C., 2012. Linking the 8.2 ka event and its freshwater forcing in the
788 Labrador Sea. Geophys Res Lett 39, L18703.

789 Hoogakker, B.A.A., Chapman, M.R., McCave, I.N., Hillaire-Marcel, C., Ellison, C.R.W.,
790 Hall, I.R., Telford, R.J., 2011. Dynamics of North Atlantic deep water masses during
791 the Holocene. Paleoceanography 26, PA4214.
792 Hu, C.Y., Henderson, G.M., Huang, J.H., Xie, S., Sun, Y., Johnson, K.R., 2008.
793 Quantification of Holocene Asian monsoon rainfall from spatially separated cave
794 records. Earth Planet Sc Lett 266, 221-232.
795 Huang, W., Chen, J.H., Zhang, X.J., Feng, S., Chen, F.H., 2015. Definition of the core zone
796 of the 'westerlies-dominated climatic regime', and its controlling factors during the
797 instrumental period. Science China: Earth Sciences 58, 676-684.
798 Issar, A., Adar, E., 2010. Progressive development of water resources in the Middle East for
799 sustainable water supply in a period of climate change. Phil Trans R Soc Lond A 368,
800 5339-5350.
801 Issar, A., Zohar, M., 2007. Climate Change: Environment and History of the Near East.
802 Springer, Berlin.
803 Ito, E., 2001. Application of Stable Isotope Techniques to Inorganic and Biogenic
804 Carbonates, in: Last, W.M., Smol, J.P. (Eds.), Tracking Environmental Change Using
805 Lake Sediments. Volume 2: Physical and Geochemical Methods. Kluwer, Dordrecht,
806 pp. 351-371.
807 Jimenez-Lopez, C., Romanek, C.S., Huertas, F.J., Ohmoto, H., Caballero, E., 2004. Oxygen
808 isotope fractionation in synthetic magnesian calcite. Geochim Cosmochim Acta 68,
809 3367-3377.
810 Jones, M.D., 2004. High-Resolution Records of Climate Change from Lacustrine Stable
811 Isotopes through the Last Two Millennia in Western Turkey. PhD, Plymouth.
812 Jones, M.D., Roberts, C.N., 2008. Interpreting lake isotope records of Holocene
813 environmental change in the Eastern Mediterranean. Quatern Int 181, 32-38.

814 Jones, M.D., Leng, M.J., Roberts, C.N., Turkes, M., Moyeed, R., 2005. A coupled calibration
815 and modelling approach to the understanding of dry-land lake oxygen isotope records. J
816 Paleolimnol 34, 391-411.
817 Jones, M.D., Roberts, C.N., Leng, M.J., 2007. Quantifying climatic change through the last
818 glacial-interglacial transition based on lake isotope palaeohydrology from central
819 Turkey. Quat Res 67, 463-473.
820 Jones, M.D., Roberts, C.N., Leng, M.J., Turkes, M., 2006. A high-resolution late Holocene
821 lake isotope record from Turkey and links to North Atlantic and monsoon climate.
822 Geology 34, 361-364.
823 Kaniewski, D., Van Campo, E., Guiot, J., Le Burel S., Otto, T., Baeteman,C., 2013.
824 Environmental roots of the Late Bronze Age Crisis. PLoS ONE 8: e71004.
825 Kelts, K., Hsu, J., 1978. Freshwater Carbonate Sedimentation, in: Lerman, A. (Ed.), Lakes:
826 Geology, Chemistry and Physics. Springer-Verlag, New York.
827 Kim, S.T., O'Neil, J.R., Hillaire-Marcel, C., Mucci, A., 2007. Oxygen isotope fractionation
828 between synthetic aragonite and water: influence of temperature and Mg2+
829 concentration. Geochim Cosmochim Acta 71, 4704-4715.
830 Kitoh, A., Yatagai, A., Alpert, P., 2008. First super-high-resolution model projection that the
831 ancient “Fertile Crescent” will disappear in this century. Hydrological Research Letters
832 2, 1-4.
833 Kotthoff, U., Koutsodendris, A., Pross, J., Schmiedl, G., Bornemann, A., Kaul, C., Marino,
834 G., Peyron, O., Schiebel, R., 2011. Impact of Lateglacial cold events on the northern
835 Aegean region reconstructed from marine and terrestrial proxy data. J Quat Sci 26, 86-
836 96.
837 Kotthoff, U., Muller, U.C., Pross, J., Schmiedl, G., Lawson, I.T., van de Schootbrugge, B.,
838 Schulz, H., 2008. Lateglacial and Holocene vegetation dynamics in the Aegean region:

839 an integrated view based on pollen data from marine and terrestrial archives. Holocene
840 18, 1019-1032.
841 Kutiel, H., Türkeş, M., 2005. New evidence for the role of the North Sea-Caspian Pattern on
842 the temperature and precipitation regimes in continental Central Turkey. Geografiska
843 Annaler Series A 87A, 501-513.
844 Kuzucuoğlu, C., Dorfler, W., Kunesch, S., Goupille, F., 2011. Mid- to late-Holocene climate
845 change in central Turkey: the Tecer Lake record. Holocene 21, 173-188.
846 Kyser, T.K., James, N.P., Bone, Y., 2002. Shallow burial dolomitization and
847 dedolomitization of Cenozoic cool-water limestones, southern Australia: geochemistry
848 and origin. J Sediment Res 72, 146-157.
849 Landmann, G., Kempe, S., 2005. Annual deposition signal versus lake dynamics: microprobe
850 analysis of Lake Van (Turkey) sediments reveals missing varves in the period 11.2-10.2
851 ka BP. Facies 51, 135-145.
852 Langgut, D., Finkelstein, I., Litt, T., 2013. Climate and the Late Bronze collapse: new
853 evidence from the southern Levant. Tel Aviv: Journal of the Institute of Archaeology of
854 Tel Aviv University 40, 149-175.
855 Leng, M.J., Jones, M.D., Frogley, M.R., Eastwood, W.J., Kendrick, C.P., Roberts, C.N.,
856 2010. Detrital carbonate influences on bulk oxygen and carbon isotope composition of
857 lacustrine sediments from the Mediterranean. Glob Planet Chang 71, 175-182.
858 Leng, M.J., Marshall, J.D., 2004. Palaeoclimate interpretation of stable isotope data from lake
859 sediment archives. Quat Sci Rev 23, 811-831.
860 Li, H.C., Ku, T.L., 1997. delta C-13-delta O-18 covariance as a paleohydrological indicator
861 for closed-basin lakes. Palaeogeogr Palaeoclimatol Palaeoecol 113, 69-80.
862 Litt, T., Ohlwein, C., Neumann, F.H., Hense, A., Stein, M., 2012. Holocene climate
863 variability in the Levant from the Dead Sea pollen record. Quat Sci Rev 49, 95-105.

Liu, Y.-H., Henderson, G.M., Hu, C.-Y., Mason, A.J., Charnley, N., Johnson, K.R., Xie, S.-C., 2013. Links between the East Asian monsoon and North Atlantic climate during the 8,200 year event. Nat Geosci 6, 117-120.

Ludwig, K.R., 2012. User's manual for Isoplot 3.75. Berkeley Geochronological Center Special Publication No. 5.

Ludwig, K.R., Titterington, D.M., 1994. Calculation of (230)Th/U isochrons, ages, and errors. Geochim Cosmochim Acta 58, 5031-5042.

Luo, S.D., Ku, T.L., 1991. U-series isochron dating - a generalized-method employing total-sample dissolution. Geochim Cosmochim Acta 55, 555-564.

Ma, Z-B., Cheng, H., Tan, M., Edwards R.L., Li, H-C., You C-F., Duan, W-H., Wang, X., Kelly M.J., 2012. Timing and structure of the Younger Dryas event in northern China. Quat Sci Rev 41, 83-93.

Mazzullo, S.J., 2000. Organogenic dolomitization in peritidal to deep-sea sediments. J Sediment Res 70, 10-23.

McCrea, J., 1950. On the isotopic chemistry of carbonates and palaeo-temperature scale. Journal of Chem Phys 18, 849-857.

Morrill, C., Jacobsen, R.M., 2005. How widespread were climate anomalies 8200 years ago? Geophys Res Lett 32, L19701.

Müller, G., Forstner, U., Irion, G., 1972. Formation and diagenesis of inorganic Ca-Mg carbonates in lacustrine environment. Naturwissenschaften 59, 158-164.

Neff, U., Burns, S.J., Mangini, A., Mudelsee, M., Fleitmann, D., Matter, A., 2001. Strong coherence between solar variability and the monsoon in Oman between 9 and 6 kyr ago. Nature 411, 290-293.

Neugebauer, I., Brauer, A., Schwab, M.J., Dulski, P., Frank, U., Hadzhiivanova, E., Kitagawa, H., Litt, T., Schiebel, V., Taha, N., Waldmann, N.D., DSDDP Scientific

889 Party. 2015. Evidences for centennial dry periods at ~3300 and ~2800 cal. Yr BP from
890 micro-facies analyses of the Dead Sea sediments. Holocene 25, 1358-1371.
891 Neumann, F.H., Kagan, E.J., Schwab, M.J., Stein, M., 2007. Palynology, sedimentology and
892 palaeoecology of the late Holocene Dead Sea. Quat Sci Rev 26, 1476-1498.
893 Ocakoğlu, F., Kir, O., Yilmaz, I.O., Acikalin, S., Erayik, C., Tunoglu, C., Leroy, S.A.G.,
894 2013. Early to mid-Holocene lake level and temperature records from the terraces of
895 Lake Sunnet in NW Turkey. Palaeogeogr Palaeoclimatol Palaeoecol 369, 175-184.
896 Ojala, A.E.K., Francus, P., Zolitschka, B., Besonen, M., Lamoureux, S.F., 2012.
897 Characteristics of sedimentary varve chronologies - a review. Quat Sci Rev 43, 45-60.
898 Ojala, A.E.K., Saarinen, T., Salonen, V.-P., 2000. Preconditions for the formation of annually
899 laminated lake sediments in southern and central Finland. Boreal Environ Res 5, 243-
900 255.
901 Orland, I.J., Edwards, R.L., Cheng, H., Kozdon, R., Cross, M., Valley, J.W., in press. Direct
902 measurements of deglacial monsoon strength in a Chinese stalagmite. Geology
903 http://www.dx.doi.org/10.1130/G36612.1
904 Orland, I.J., Bar-Matthews, M., Kita, N.T., Ayalon, A., Matthews, A., Valley, J.W., 2009.
905 Climate deterioration in the Eastern Mediterranean as revealed by ion microprobe
906 analysis of a speleothem that grew from 2.2 to 0.9 ka in Soreq Cave, Israel. Quat Res
907 71, 27-35.
908 Peyron, O., Goring, S., Dormoy, I., Kotthoff, U., Pross, J., De Beaulieu, J.L., Drescher-
909 Schneider, R., Vanniere, B., Magny, M., 2011. Holocene seasonality changes in the
910 central Mediterranean region reconstructed from the pollen sequences of Lake Accesa
911 (Italy) and Tenaghi Philippon (Greece). Holocene 21, 131-146.

912 Prasad, S., Vos, H., Negendank, J.F.W., Waldmann, N., Goldstein, S.L., Stein, M., 2004.
913 Evidence from Lake Lisan of solar influence on decadal- to centennial-scale climate
914 variability during marine oxygen isotope stage 2. Geology 32, 581-584.
915 Raicich, F., Pinardi, N., Navarra, A., 2003. Teleconnections between Indian monsoon and
916 Sahel rainfall and the Mediterranean. Int J Climatol 23, 173-186.
917 Rasmussen, S.O., Andersen, K.K., Svensson, A.M., Steffensen, J.P., Vinther, B.M., Clausen,
918 H.B., Siggaard-Andersen, M.L., Johnsen, S.J., Larsen, L.B., Dahl-Jensen, D., Bigler,
919 M., Rothlisberger, R., Fischer, H., Goto-Azuma, K., Hansson, M.E., Ruth, U., 2006. A
920 new Greenland ice core chronology for the last glacial termination. J Geophys Res-
921 Atmos 111, 1-16.
922 Renssen, H., Brovkin, V., Fichefet, T., Goosse, H., 2006. Simulation of the Holocene climate
923 evolution in Northern Africa: the termination of the African Humid Period. Quat Int
924 150, 95-102.
925 Renssen, H., Goosse, H., Fichefet, T., 2007. Simulation of Holocene cooling events in a
926 coupled climate model. Quat Sci Rev 26, 2019-2029.
927 Roberts, N., Eastwood, W.J., Kuzucuoğlu, C., Fiorentino, G., Caracuta, V., 2011. Climatic,
928 vegetation and cultural change in the eastern Mediterranean during the mid-Holocene
929 environmental transition. Holocene 21, 147-162.
930 Roberts, N., Jones, M.D., Benkaddour, A., Eastwood, W.J., Filippi, M.L., Frogley, M.R.,
931 Lamb, H.F., Leng, M.J., Reed, J.M., Stein, M., Stevens, L., Valero-Garces, B.,
932 Zanchetta, G., 2008. Stable isotope records of Late Quaternary climate and hydrology
933 from Mediterranean lakes: the ISOMED synthesis. Quat Sci Rev 27, 2426-2441.
934 Roberts, N., Reed, J.M., Leng, M.J., Kuzucuoğlu, C., Fontugne, M., Bertaux, J., Woldring,
935 H., Bottema, S., Black, S., Hunt, E., Karabiyikoglu, M., 2001. The tempo of Holocene

climatic change in the eastern Mediterranean region: new high-resolution crater-lake sediment data from central Turkey. Holocene 11, 721-736.

Rohling, E.J., Pälike, H., 2005. Centennial-scale climate cooling with a sudden cold event around 8,200 years ago. Nature 434, 975-979.

Rosen, A., 2007. Civilizing Climate. AltaMira Press, Plymouth.

Rowe, P.J., Mason, J.E., Andrews, J.E., Marca, A.D., Thomas, L., van Calsteren, P., Jex, C.N., Vonhof, H.B., Al-Omari, S., 2012. Speleothem isotopic evidence of winter rainfall variability in northeast Turkey between 77 and 6 ka. Quat Sci Rev 45, 60-72.

Sabins, F.F., 1962. Grains of detrital, secondary, and primary dolomite from Cretaceous Strata of the western interior. Geological Society of America Bulletin 73, 1183-1196.

Sahy, D., Cremiere, A., Lepland, A., Noble, S.R., Condon, D., Brunstad, H., 2014. Tempo of methane derived authigenic carbonate formation from the North Sea and the Barents Sea. Geological Society of America annual meeting, Vancouver, British Columbia, paper 252-7.

Schilman, B., Bar-Matthews, M., Almogi-Labin, A., Luz, B., 2001. Global climate instability reflected by Eastern Mediterranean marine records during the late Holocene. Palaeogeogr Palaeoclimatol Palaeoecol176, 157-176.

Schneider, T., Bischoff, T., Haug, G.H., 2014. Migrations and dynamics of the intertropical convergence zone. Nature 513, 45-53.

Shakun, J.D., Burns, S.J., Fleitmann, D., Kramers, J., Matter, A., Al-Subary, A., 2007. A high-resolution, absolute-dated deglacial speleothem record of Indian Ocean climate from Socotra Island, Yemen. Earth Planet Sc Lett 259, 442-456.

Sharp, Z., 2007. Stable Isotope Geochemistry. Pearson, New Jersey.

959 Stanley, J.D., Krom, M.D., Cliff, R.A., Woodward, J.C., 2003. Short contribution: Nile flow
960 failure at the end of the old kingdom, Egypt: Strontium isotopic and petrologic
961 evidence. Geoarchaeology 18, 395-402.
962 Stevens, L.R., Ito, E., Schwalb, A., Wright, H.E., 2006. Timing of atmospheric precipitation
963 in the Zagros Mountains inferred from a multi-proxy record from Lake Mirabad, Iran.
964 Quat Res 66, 494-500.
965 Stevens, L.R., Wright, H.E., Ito, E., 2001. Proposed changes in seasonality of climate during
966 the Lateglacial and Holocene at Lake Zeribar, Iran. Holocene 11, 747-755.
967 Talbot, M., 1990. A review of the palaeohydrological interpretation of carbon and oxygen
968 isotopic ratios in primary lacustrine carbonates. Chem Geol 80, 261-279.
969 Tarutani, T., Clayton, R.N., Mayeda, T.K., 1969. The effect of polymorphims and
970 magnesium substitution on oxygen isotope fractionation between calcium carbonate
971 and water. Geochim Cosmochim Acta 33, 987-996.
972 Teller, J.T., 2012. Importance of freshwater injections into the Arctic Ocean in triggering the
973 Younger Dryas cooling. PNAS 109, 19880-19881.
974 Thomas, E.R., Wolff, E.W., Mulvaney, R., Steffensen, J.P., Johnsen, S.J., Arrowsmith, C.,
975 White, J.W.C., Vaughn, B., Popp, T., 2007. The 8.2 ka event from Greenland ice cores.
976 Quat Sci Rev 26, 70-81.
977 Turner, R., Roberts, N., Eastwood, W.J., Jenkins, E., Rosen, A., 2010. Fire, climate and the
978 origins of agriculture: micro-charcoal records of biomass burning during the last
979 glacial-interglacial transition in Southwest Asia. J Quat Sci 25, 371-386.
980 Turner, R., Roberts, N., Jones, M.D., 2008. Climatic pacing of Mediterranean fire histories
981 from lake sedimentary microcharcoal. Glob Planet Chang 63, 317-324.
982 Türkeş, M., Koc, T., Saris, F., 2009. Spatiotemporal variability of precipitation total series
983 over Turkey. Int J Climatol 29, 1056-1074

Tyrlis, E., Lelieveld, J., Steil, B., 2013. The summer circulation over the eastern Mediterranean and the Middle East: influence of the South Asian monsoon. Clim Dyn 40, 1103-1123.

Tzedakis, P.C., 2007. Seven ambiguities in the Mediterranean palaeoenvironmental narrative. Quat Sci Rev 26, 2042-2066.

Ulgen, U.B., Franz, S.O., Biltekin, D., Cagatay, M.N., Roeser, P.A., Doner, L., Thein, J., 2012. Climatic and environmental evolution of Lake Iznik (NW Turkey) over the last similar to 4700 years. Quat Int 274, 88-101.

Vanniere, B., Power, M.J., Roberts, N., Tinner, W., Carrion, J., Magny, M., Bartlein, P., Colombaroli, D., Daniau, A.L., Finsinger, W., Gil-Romera, G., Kaltenrieder, P., Pini, R., Sadori, L., Turner, R., Valsecchi, V., Vescovi, E., 2011. Circum-Mediterranean fire activity and climate changes during the mid-Holocene environmental transition (8500-2500 cal. BP). Holocene 21, 53-73.

Vasconcelos, C., McKenzie, J.A., 1997. Microbial mediation of modern dolomite precipitation and diagenesis under anoxic conditions (Lagoa Vermelha, Rio de Janeiro, Brazil). J Sediment Res 67, 378-390.

Verheyden, S., Nader, F.H., Cheng, H.J., Edwards, L.R., Swennen, R., 2008. Paleoclimate reconstruction in the Levant region from the geochemistry of a Holocene stalagmite from the Jeita cave, Lebanon. Quat Res 70, 368-381.

Vinther, B.M., Clausen, H.B., Johnsen, S.J., Rasmussen, S.O., Andersen, K.K., Buchardt, S.L., Dahl-Jensen, D., Seierstad, I.K., Siggaard-Andersen, M.L., Steffensen, J.P., Svensson, A., Olsen, J., Heinemeier, J., 2006. A synchronized dating of three Greenland ice cores throughout the Holocene. J Geophys Res-Atmos 111, D13102.

1007 von Grafenstein, U., Erlenkeuser, H., Brauer, A., Jouzel, J., Johnsen, S.J., 1999. A mid-
1008 European decadal isotope-climate record from 15,500 to 5000 years BP. Science 284,
1009 1654-1657.
1010 Wang, Y.J., Cheng, H., Edwards, R.L., An, Z.S., Wu, J.Y., Shen, C.C., Dorale, J.A., 2001. A
1011 high-resolution absolute-dated Late Pleostocene monsoon record from Hulu Cave
1012 China. Science 294, 2345-2348.
1013 Weiss, B., 1982. The decline of Late Bronze-Age civilization as a possible response to
1014 climatic-change. Clim Chang 4, 173-198.
1015 Weiss, H., 1993. The genesis and collapse of thirs millennium north Mesopotamian
1016 civilisation. Science 261, 995-1004.
1017 Wick, L., Lemcke, G., Sturm, M., 2003. Evidence of Lateglacial and Holocene climatic
1018 change and human impact in eastern Anatolia: high-resolution pollen, charcoal, isotopic
1019 and geochemical records from the laminated sediments of Lake Van, Turkey. Holocene
1020 13, 665-675.
1021 Wiersma, A.P., Renssen, H., 2006. Model-data comparison for the 8.2 ka BP event:
1022 confirmation of a forcing mechanism by catastrophic drainage of Laurentide Lakes.
1023 Quat Sci Rev 25, 63-88.
1024 Wilson, G.P., Reed, J.M., Lawson, I.T., Frogley, M.R., Preece, R.C., Tzedakis, P.C., 2008.
1025 Diatom response to the Last Glacial-Interglacial Transition in the Ioannina basin,
1026 northwest Greece: implications for Mediterranean palaeoclimate reconstruction. Quat
1027 Sci Rev 27, 428-440.
1028 Woodbridge, J., Roberts, N., 2011. Late Holocene climate of the Eastern Mediterranean
1029 inferred from diatom analysis of annually-laminated lake sediments. Quat Sci Rev 30,
1030 3381-3392.

1031 Yu, S.Y., Colman, S.M., Lowell, T.V., Milne, G.A., Fisher, T.G., Breckenridge, A., Boyd,
1032 M., Teller, J.T., 2010. Freshwater outburst from Lake Superior as a trigger for the cold
1033 event 9300 years ago. Science 328, 1262-1266.
1034 Ziv, B., Dayan, U., Kushnir, Y., Roth, C., Enzel, Y., 2006. Regional and global atmospheric
1035 patterns governing rainfall in the southern Levant. Int J Climatol 26, 55-73.
1036 Zolitschka, B., Francus, P., Ojala, A.E.K., Schimmelmann, A., 2015. Varves in lake
1037 sediments - a review. Quat Sci Rev 117, 1-41.

Figure captions *(all figures black and white only)*

Figure 1 Location of Nar Gölü in central Turkey, and the lake, ice and cave sites from which key isotope records referred to in this study have been produced.

Figure 2 Age-depth plot for the NAR01/02 and NAR10 master sequences. The NAR01/02 chronology was constructed using varve counts (Jones et al., 2005), and the NAR10 chronology using a mixture of varve counts and two U-Th dates. We use linear interpolation for the non-varved sections 598-754 and 1965-2053 cm, and this is signified on the plot by the dashed lines. Depths for the NAR01/02 sequence are approximate, as they were taken by varve year, not against depth. The sections where there were gaps due to coring are shown by the white boxes.

Figure 3 $\delta^{18}O_{carbonate}$ and $\delta^{13}C_{carbonate}$ data plotted against depth, with the locations of varved and non-varved sediments and carbonate mineralogy also shown. Relatively few samples are a mixture of aragonite and calcite, such that >50% calcite is defined as calcite and >50% aragonite as aragonite. Where dolomite is present, samples are shown as containing >20% dolomite (those samples not run for isotopes) and <20% dolomite (those samples run using the selective reaction method). Depths for the NAR01/02 sequence are approximate, as they were taken by varve year, not against depth.

Figure 4 $\delta^{18}O_{carbonate}$ record for the late glacial to Holocene transition at Nar Gölü, with the varved section up to the second youngest sample analysed at 3-year resolution. Shifts between aragonite and calcite are also shown.

Figure 5 $\delta^{18}O_{carbonate}$ records from Nar Gölü and other sites in the Eastern Mediterranean arranged in increasing distance from Nar Gölü, with more positive values indicating drier conditions: Eski Acıgöl (Roberts et al., 2001), Gölhisar Gölü (Eastwood et al., 2007), Soreq Cave (Bar-Matthews et al., 1997; 1999; Orland et al., 2009; Bar-Matthews and Ayalon, 2011), Lake Van (core 90-4, 20-year interpolated values) (Wick et al., 2003) and Lake Zeribar (Stevens et al., 2001). All records show a transition in the mid Holocene to more positive values. The chronology at Nar Gölü further back in time than the point marked with the asterisk (*) is very tentative and based on comparison to NGRIP; we are careful not to over-interpret this period in the discussion. The sections where there were gaps due to coring or where isotope data are not shown due to the issues with the chronology (section 4.1) are shown by the white boxes.

Figure 6 Nar Gölü $\delta^{18}O$ data for the late glacial and early Holocene, compared to records from further east in Asia, and the North Atlantic: Qunf in Oman (Fleitmann et al., 2003; 2007), Kulishu (Ma et al., 2012), Dongge (Dykoski et al., 2005), Heshang (Hu et al., 2008; Liu et al., 2013) and Hulu (H82) (Wang et al., 2001) caves in China, Ammersee in Germany (reversed scale) (von Grafenstein et al., 1999) and NGRIP (reversed scale) (Vinther et al., 2006; Rasmussen et al., 2006). While there are rapid transitions into the Holocene in Nar Gölü, some records from China, as well as North Atlantic records, the difference is greater during the early Holocene 'events', where many records further away from the North Atlantic have less discrete and longer anomalies than the shorter 9.3 and 8.2 ka events in the North Atlantic region.


NGRIP
Ammersee
Nar Gölü
Van
Soreq
Qunf
Moomi
Kulishu
Hulu
Heshang
Dongge

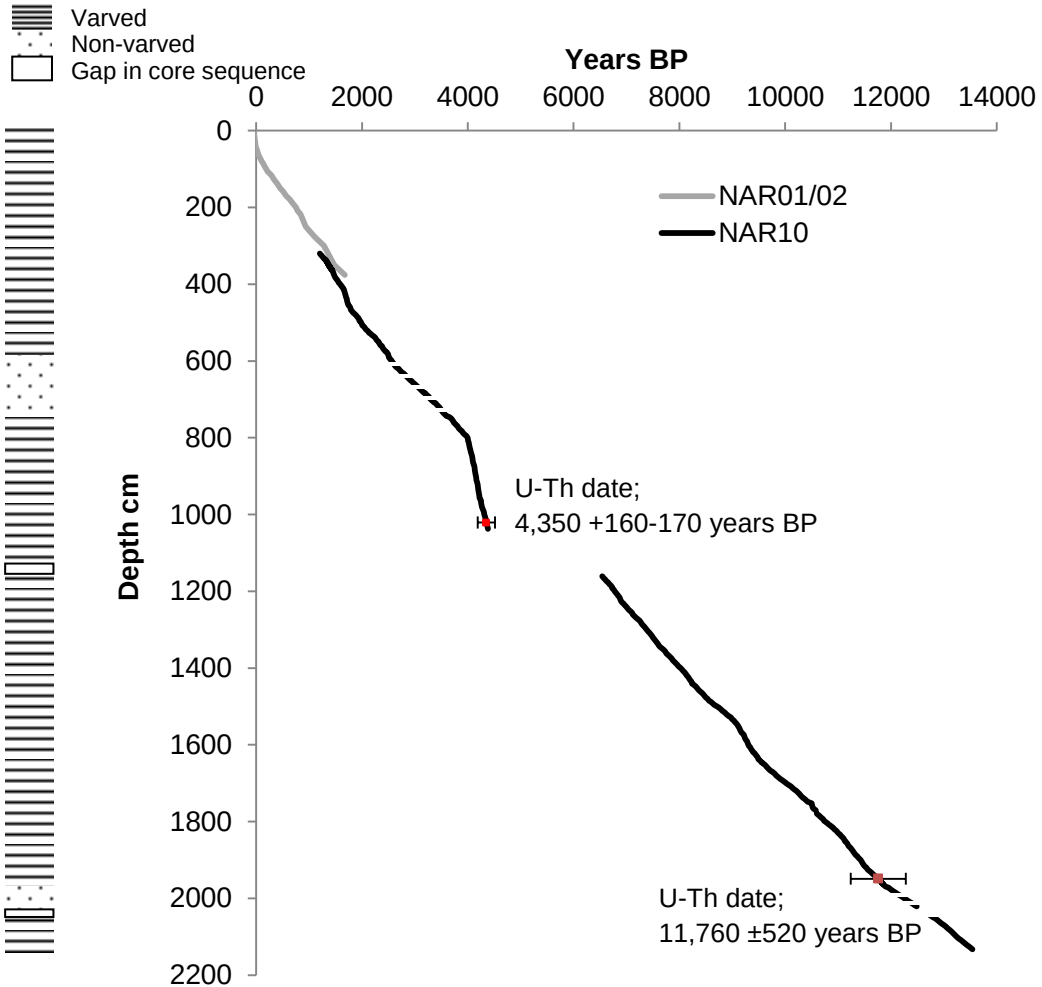
Varved
Non-varved
Gap in core sequence
Years BP
0
2000
4000
6000
8000
10000
12000
14000
Depth cm
0
200
400
600
800
1000
1200
1400
1600
1800
2000
2200
NAR01/02
NAR10
U-Th date;
4,350 +160-170 years BP
U-Th date;
11,760 ±520 years BP

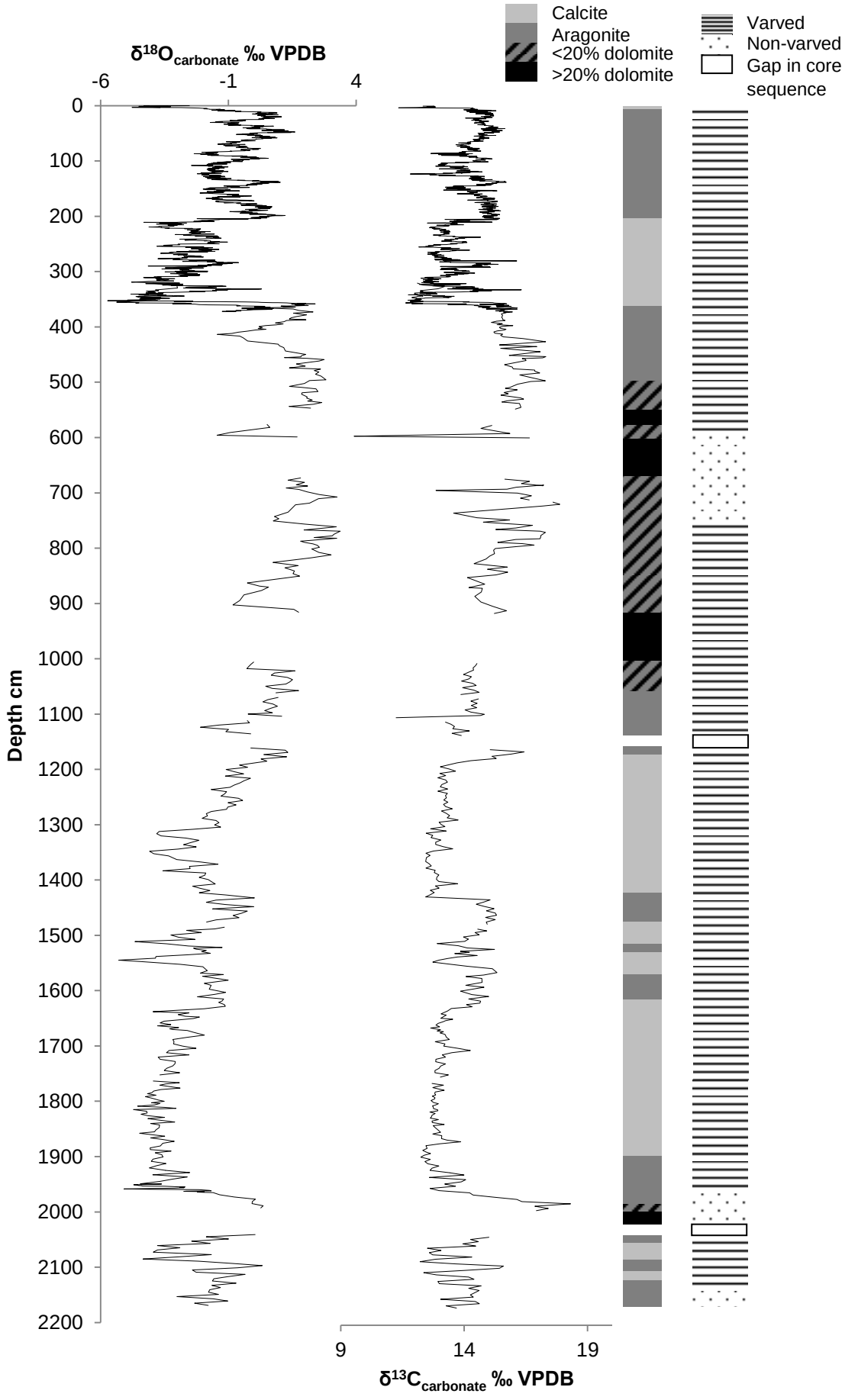
Calcite
Aragonite
<20% dolomite
>20% dolomite
Varved
Non-varved
Gap in core sequence
δ18Ocarbonate ‰ VPDB
-6
-1
4
Depth cm
0
100
200
300
400
500
600
700
800
900
1000
1100
1200
1300
1400
1500
1600
1700
1800
1900
2000
2100
2200
9
14
19
δ13Ccarbonate ‰ VPDB

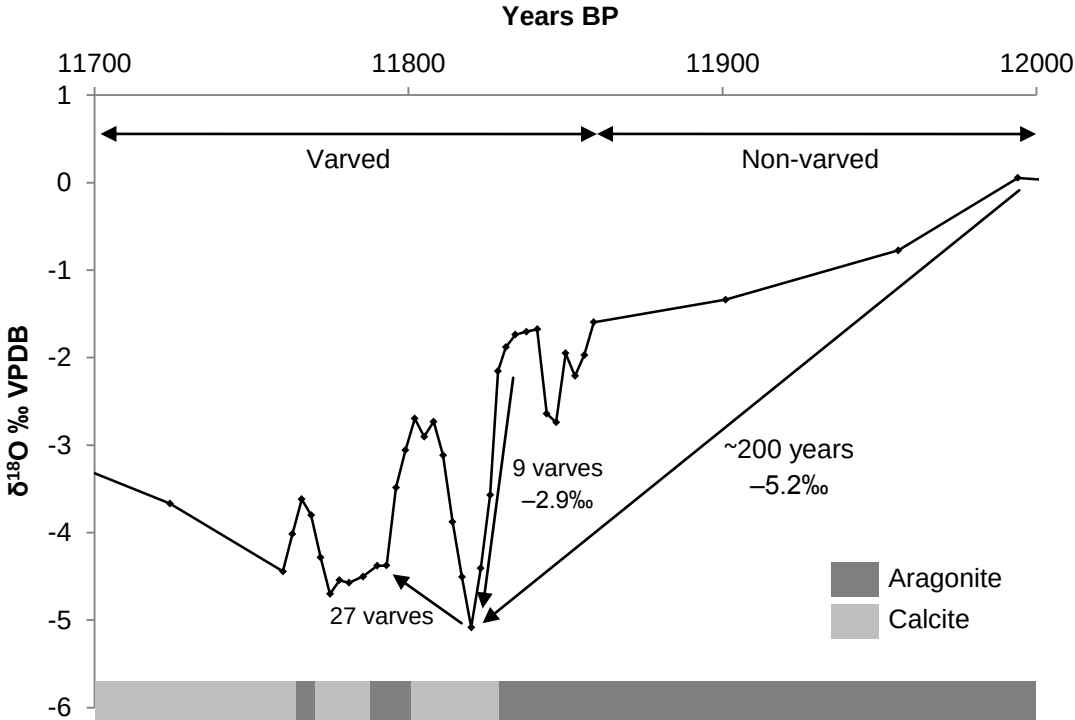
Years BP
11700
11800
11900
12000
1
0
-1
-2
-3
-4
-5
-6
δ18O ‰ VPDB
Varved
Non-varved
9 varves
–2.9‰
~200 years
–5.2‰
27 varves
Aragonite
Calcite

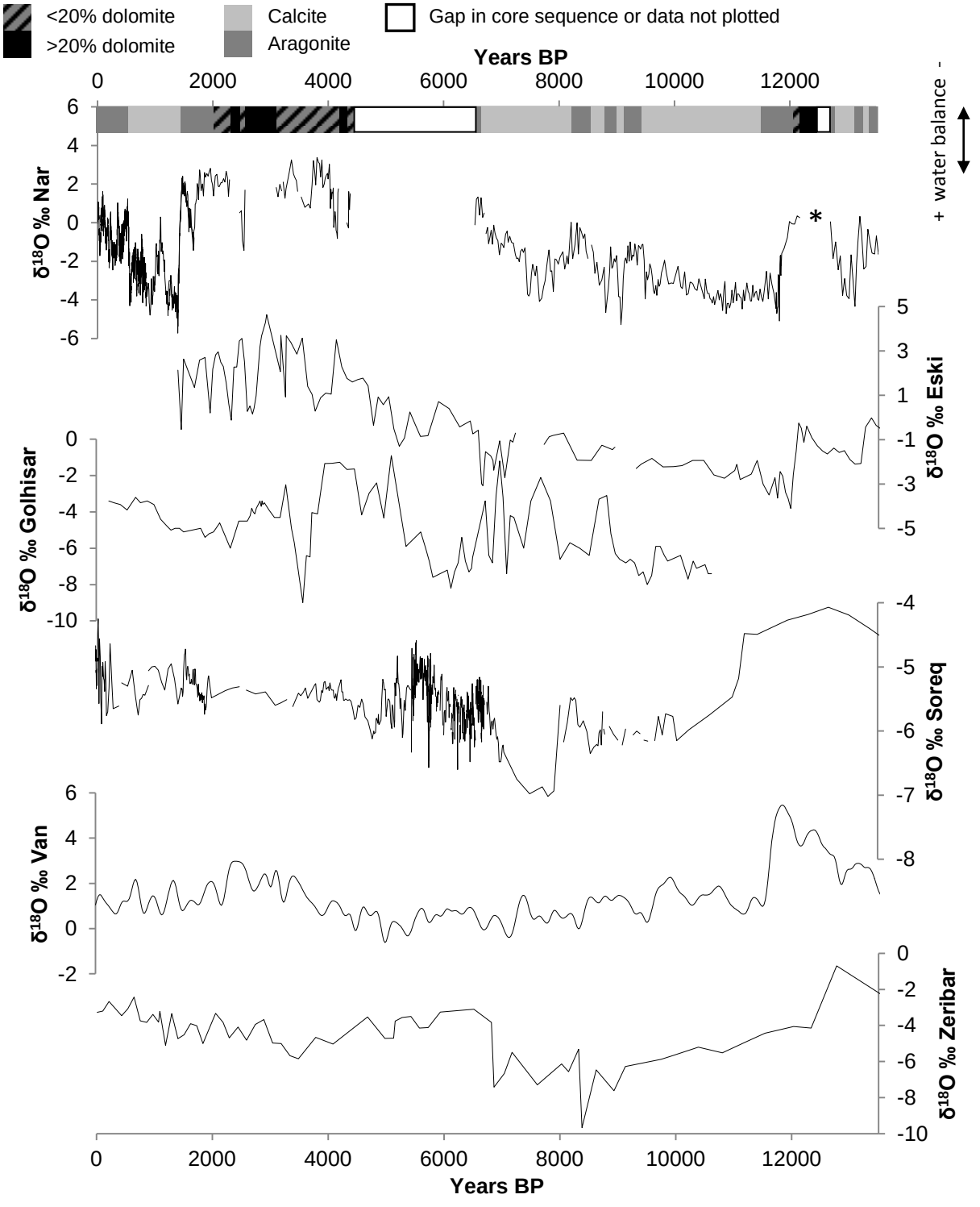
<20% dolomite
>20% dolomite
Calcite
Aragonite
Gap in core sequence or data not plotted
Years BP
0
2000
4000
6000
8000
10000
12000
+ water balance -
δ18O ‰ Nar
δ18O ‰ Eski
δ18O ‰ Golhisar
δ18O ‰ Soreq
δ18O ‰ Van
δ18O ‰ Zeribar
*

8.2ka event
9.3ka event
Transition into Holocene
Years BP
7000
8000
9000
10000
11000
12000
δ18O ‰ Nar
+ water balance -
δ18O ‰ Qunf
+ monsoon intensity -
δ18O ‰ Kulishu
+ monsoon intensity -
δ18O ‰ Dongge
+ monsoon intensity -
δ18O ‰ Heshang
+ monsoon intensity -
δ18O ‰ Hulu
+ monsoon intensity -
δ18O ‰ Ammersee
Warmer Cooler
δ18O ‰ NGRIP
Warmer Cooler

Table A.1 U-Th data from NAR10 core sequence. Decay constants from Cheng et al. 2013 are used for calculation of activity ratios. All uncertainties are ± 2s % and absolute as noted. Detrital Th corrected data use an average continental detritus composition. Dates shown are calculated for data with and without detrital Th correction (years before date of analysis), and for detrital Th-corrected data in years BP.

			Measured, Tracer-Corrected							Detrital-Corrected											
Sample	U ppm	232Th ppm	230 /232 AR	232 /238 AR	±2s (%)	230 /238 AR	±2s (%)	234 /238 AR	±2s (%)	230Th/ 238U AR	±2s (%)	234U/ 238U AR	±2s (%)	Corr. Coef. 08-48	Date uncorr (ka)	±2s (abs)	Date corr (ka)	Date corr (ka BP)	±2s (abs)	Initial 234U/ 238U AR	±2s (abs)
760 cm A	0.2833	0.3055	1.03	0.3543	0.35	0.3640	0.45	1.148	0.14	0.09756	11.52	1.211	0.43	-0.40	41.20	0.32	9.141	9.078	1.106	1.216	±0.005
760 cm C	0.1252	0.3244	0.97	0.8516	0.35	0.8239	0.43	1.094	0.17	0.3936	11.70	1.325	2.37	-0.50	147.4	4.10	37.85	37.79	5.824	1.362	±0.032
900 cm A	0.2969	0.3862	1.02	0.4275	0.35	0.4362	0.43	1.247	0.14	0.1243	11.61	1.384	0.61	-0.61	46.21	0.37	10.22	10.15	1.271	1.395	±0.008
900 cm C	0.2024	0.6999	0.90	1.1361	0.36	1.019	0.42	1.094	0.14	1.354	16.61	2.759	31.35	0.81	261.7	34	67.96	67.90	18.731	3.131	±0.949
1070 cm A	0.2362	0.2516	1.07	0.3502	0.30	0.3751	0.43	1.358	0.16	0.1176	9.21	1.506	0.50	-0.67	34.73	0.24	8.828	8.765	0.871	1.518	±0.007
1070 cm D	0.2354	0.0903	1.40	0.1260	0.30	0.1759	0.51	1.425	0.15	0.07920	4.16	1.475	0.21	-0.43	14.27	0.09	6.000	5.937	0.261	1.483	±0.003
715 cm A	0.2370	0.6414	0.96	0.8894	0.31	0.8499	0.48	1.050	0.20	0.4202	12.42	1.192	2.54	-0.28	176.3	8.0	46.78	46.71	7.721	1.219	±0.033
715 cm D	0.1885	0.2592	1.04	0.4519	0.30	0.4683	0.45	1.168	0.17	0.1472	10.44	1.270	0.63	-0.47	55.09	0.51	13.38	13.31	1.518	1.280	±0.008
1949 cm A	0.4348	0.1270	2.25	0.09599	0.08	0.2162	0.31	1.277	0.19	0.1480	1.53	1.301	0.22	-0.21	20.09	0.09	13.11	13.05	0.221	1.312	±0.003
1949 cm B	0.4741	0.1248	2.38	0.08653	0.06	0.2058	0.26	1.281	0.15	0.1441	1.40	1.302	0.18	-0.23	18.99	0.07	12.73	12.67	0.195	1.313	±0.002
1949 cm C	0.3048	0.1261	1.82	0.1360	0.05	0.2475	0.31	1.265	0.14	0.1513	2.15	1.298	0.20	-0.33	23.57	0.10	13.45	13.39	0.318	1.310	±0.003
1949 cm D	3.179	1.4969	1.70	0.1547	0.06	0.2632	0.27	1.267	0.14	0.1541	2.41	1.307	0.21	-0.38	25.17	0.10	13.62	13.55	0.361	1.319	±0.003
1949 cm E	0.3310	0.1613	1.69	0.1602	0.24	0.2703	0.41	1.266	0.15	0.1579	2.52	1.307	0.23	-0.36	25.97	0.14	13.98	13.91	0.387	1.319	±0.003
1021 cm A	1.542	1.303	1.07	0.2778	0.07	0.2984	0.35	1.371	0.12	0.08711	9.26	1.483	0.36	-0.66	26.46	0.13	6.580	6.517	0.643	1.492	±0.005
1021 cm B	1.474	2.210	0.98	0.4925	0.07	0.4836	0.27	1.290	0.12	0.1242	14.34	1.492	0.79	-0.71	50.25	0.28	9.433	9.370	1.462	1.505	±0.011
1021 cm C	1.660	3.050	0.96	0.6038	0.07	0.5799	0.31	1.252	0.11	0.1543	16.29	1.508	1.14	-0.72	66.16	0.50	11.71	11.64	2.105	1.525	±0.016
1021 cm D	1.671	3.318	0.95	0.6524	0.09	0.6217	0.29	1.234	0.11	0.1711	16.95	1.513	1.34	-0.72	74.39	0.60	13.00	12.94	2.463	1.532	±0.018
1021 cm E	2.171	3.072	0.98	0.4651	0.08	0.4580	0.38	1.300	0.13	0.1151	14.32	1.489	0.72	-0.70	46.53	0.34	8.732	8.669	1.343	1.502	±0.010
0 age core A	0.1339	2.012	0.83	4.937	0.08	4.106	0.26	1.052	0.14												
0 age core B	0.9815	4.077	0.84	1.365	0.19	1.142	0.32	0.9985	0.15												
0 age core C	0.6091	2.299	0.83	1.240	0.09	1.033	0.28	1.010	0.13												
0 age core D	0.4700	1.569	0.84	1.097	0.11	0.9242	0.30	1.026	0.15												
0 age core E	1.019	4.198	0.83	1.354	0.21	1.117	0.34	0.9978	0.13												

1 ka (305 cm) A	0.6956	2.075	0.84	0.9802	0.20	0.8282	0.35	1.134	0.15
1 ka (305 cm) B	0.3764	1.114	0.84	0.9725	0.08	0.8140	0.35	1.121	0.14
1 ka (305 cm) C	0.4119	1.235	0.84	0.9852	0.09	0.8278	0.28	1.122	0.16
1 ka (305 cm) D	0.4003	1.237	0.83	1.015	0.08	0.8437	0.28	1.116	0.15
1 ka (305 cm) E	0.8744	2.748	0.85	1.033	0.12	0.8738	0.29	1.131	0.15
Turbidite A	2.066	10.92	0.85	1.737	0.60	1.473	0.66	0.9834	0.29
Turbidite B	2.393	11.37	0.84	1.562	0.66	1.308	0.71	0.9816	0.25
Turbidite C	2.443	10.78	0.89	1.450	0.27	1.296	0.37	0.9818	0.13
Turbidite D	1.407	7.134	0.85	1.666	0.56	1.424	0.62	0.9799	0.17

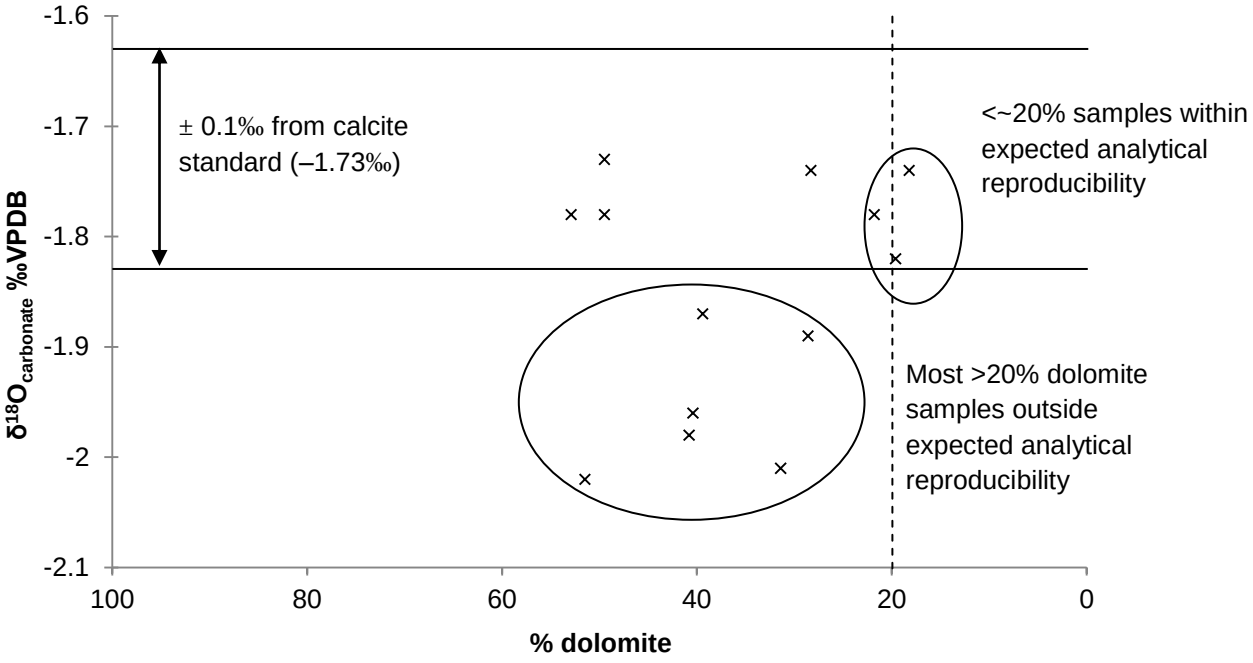

Figure A.1 δ^{18}O of samples reacted at 16°C for 1 hour containing mixtures of dolomite and calcite standards. Samples with <20% dolomite were all within expected analytical reproducibility.

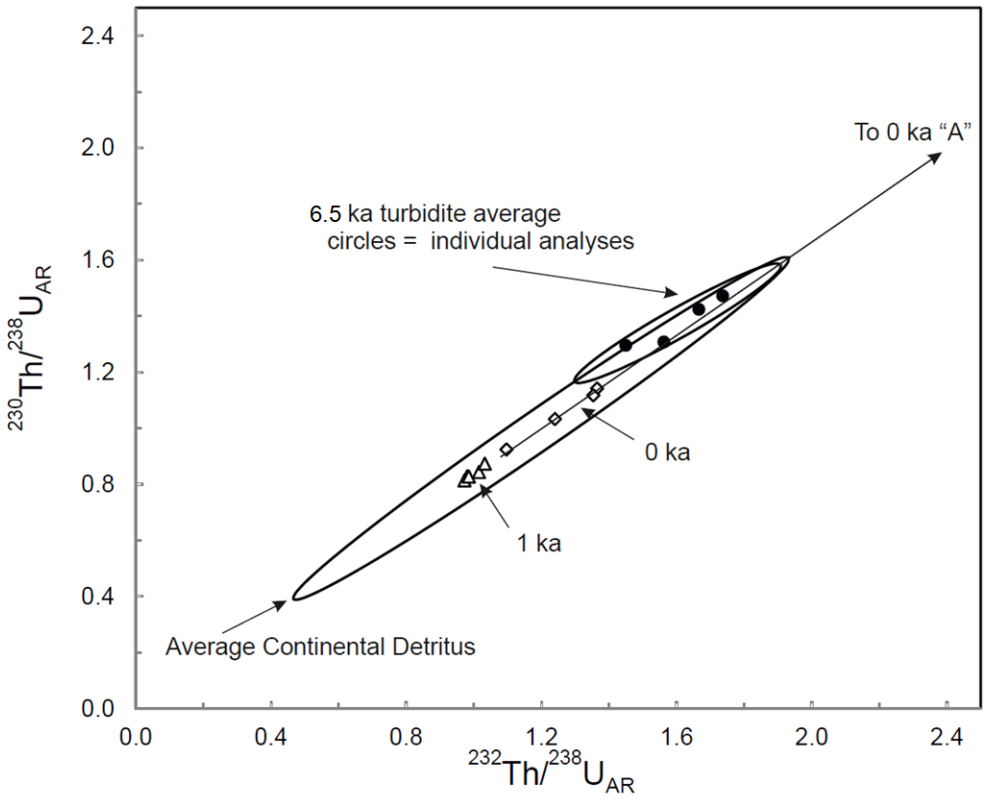

Figure A.2 $^{230}Th/^{238}U$ $^{232}Th/^{238}U$ plot of detritus and carbonates from the sediment core of known ages. Sub sample A from 0ka plots off the graph, indicated by the arrow marked "To 0ka A", but still in a line with the other samples.

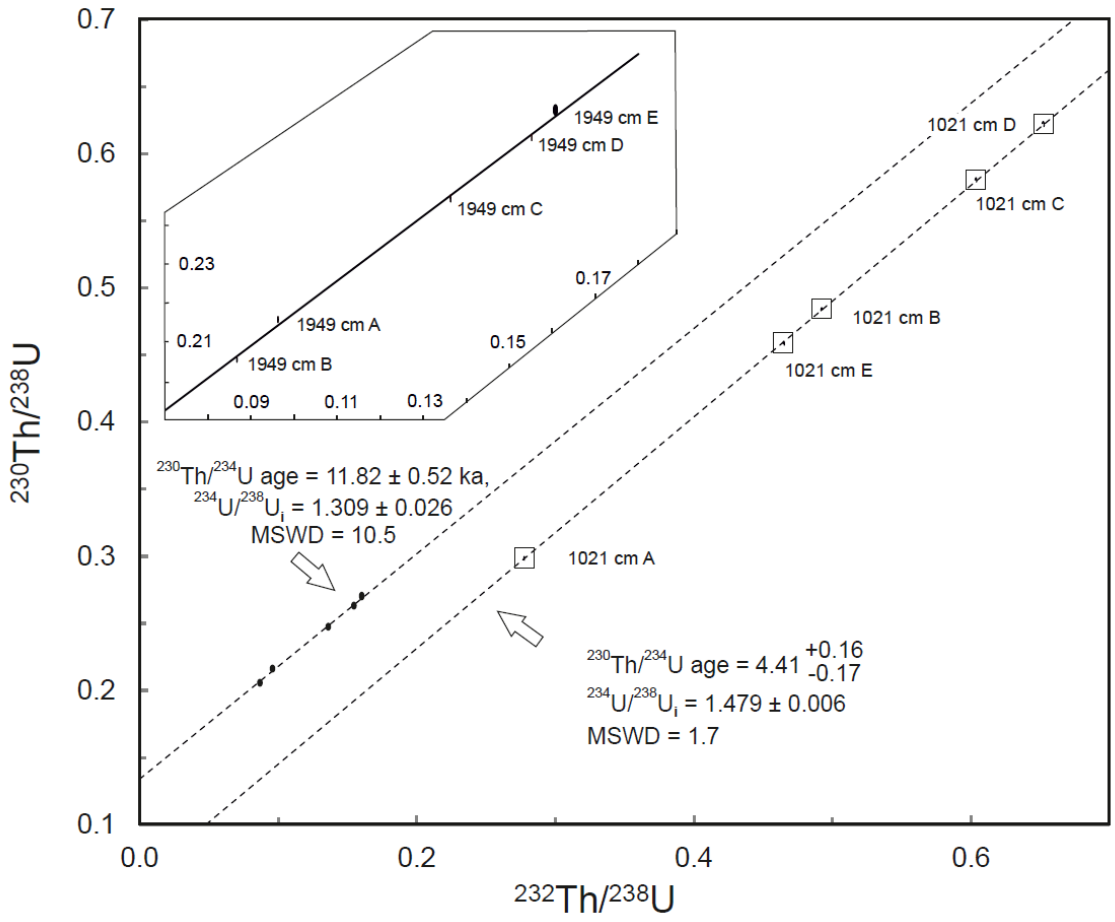

Figure A.3 2D projection of the 3D ^{230}Th/U isochron (Ludwig and Titterington, 1994), with 2 sigma uncertainty ellipses. The ellipses are small for the 1021 cm sample so are highlighted with boxes. A magnification of the isochron for 1949 cm is shown inset.

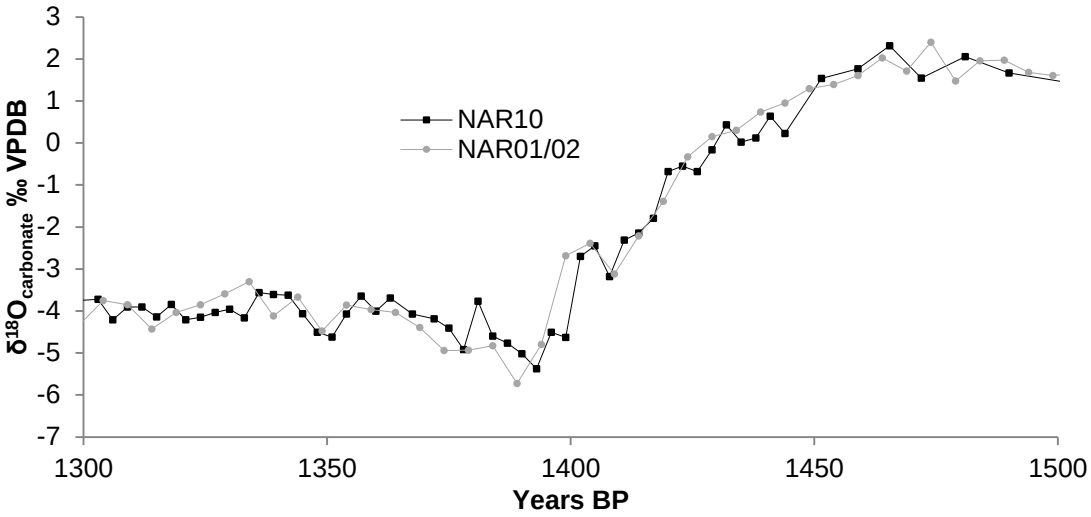

Figure A.4 Comparison of $\delta^{18}O_{carbonate}$ data from NAR10 and NAR01/02 cores through a major late Holocene climatic transition. There is very little apparent offset between the two records.

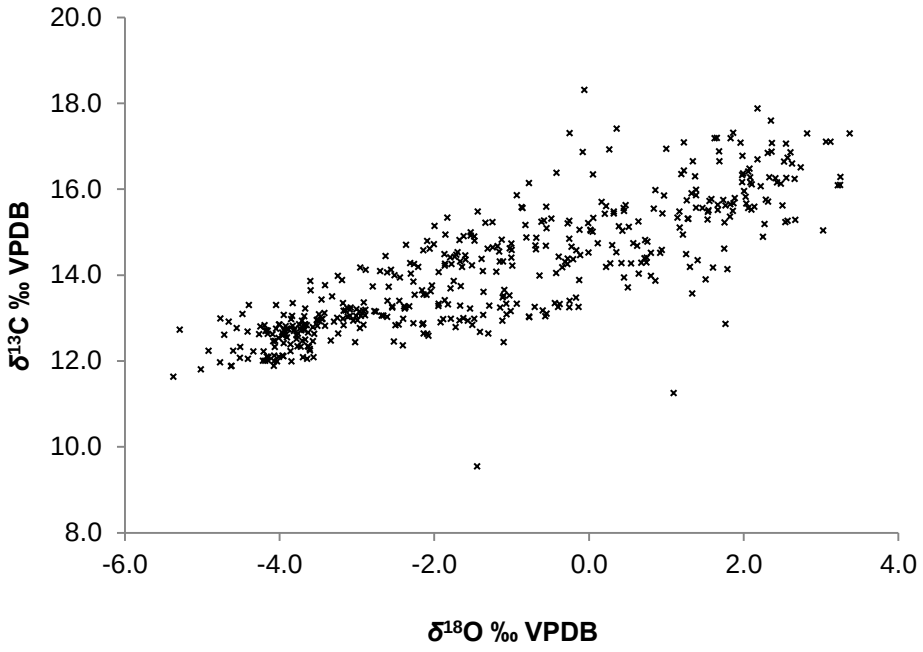

Figure A.5 $\delta^{13}C_{carbonate}$ data from the NAR10 core sequence plotted against $\delta^{18}O_{carbonate}$.

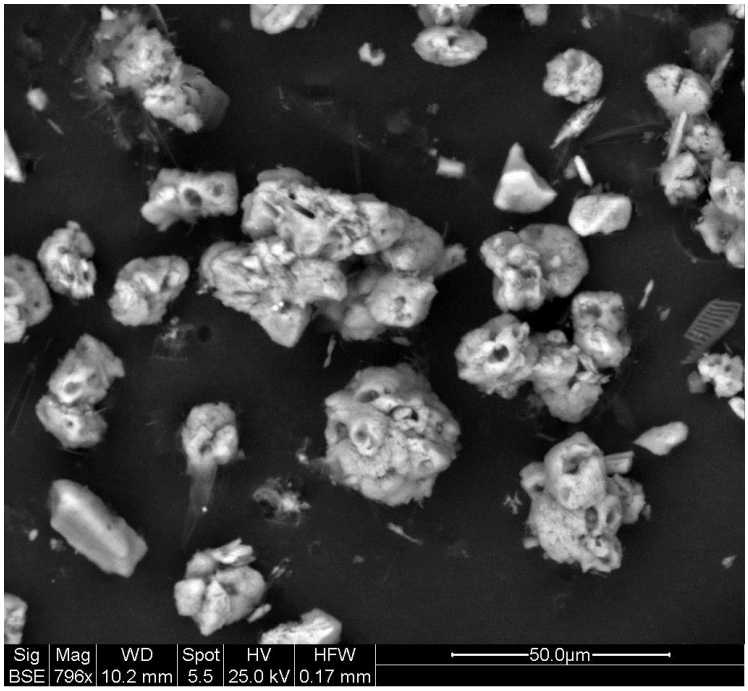

Figure A.6 Dolomite crystals viewed under SEM, showing non-rhombic shapes and microstructures, suggesting a diagenetic origin.